ASCE J. ENGINEERING MECHANICS

https://ascelibrary.org/journal/jenmdt

ISSN (print): 0733-9399 | ISSN (online): 1943-7889

IMPACT FACTOR = 2.35

Editor: Prof. Roberto Ballarini, Ph.D., P.E., FASCE, University of Houston, Texas, USA.

Accepted November 22nd 2020

LINEAR STABILITY ANALYSIS AND CFD SIMULATION OF THERMAL "VISCOUS FINGERING" INSTABILITY IN ANISOTROPIC POROUS MEDIA

M. Norouzi[1,*], S. Dorrani[2], H. Shokri[3] and **O. Anwar Bég[4]**

[1] Associate Professor, Mechanical Engineering Department, Shahrood University of Technology, Shahrood, Iran, Email: mnorouzi@shahroodut.ac.ir
[2]Mechanical Engineering Department, Shahrood University of Technology, Shahrood, Iran, Email: sedigh.dorrani@yahoo.com
[3]Mechanical Engineering Department, Shahrood University of Technology, Shahrood, Iran, Email: hosnashokri@gmail.com
[4] Professor, Multi-Physical Engineering Sciences Group (MPESG), Mechanical and Aeronautical Engineering Dept. School of , Salford University, M54WT, **UK.** Email: O.A.Beg@salford.ac.uk

ABSTRACT

The water or steam injection in oil fields is a usual method for enhanced oil recovery in petroleum engineering. The thermo-viscous fingering instability is one of the main problems with complex nature that decreases the efficiency of oil extraction. Actually, the oil wells are the porous medium with a level of anisotropy for permeability and diffusion. In this paper, the thermal viscous fingering instability in anisotropic media has been investigated using both linear stability analysis and CFD simulation. For stability analysis, the growth rate of disturbances is determined by solving quasi-steady state equations via shooting method. The CFD simulation is performed by solving the governing equations of heat and mass transfer using a spectral method. It is shown that the longitudinal direction permeability and the transverse direction dispersion have important effect on the instability. The value of thermal-lag coefficient and the Lewis number have opposite effects on the different types of displacements that are considered. For the case of sweeping the porous media via the cold fluid, increasing the Lewis number intensifies the level of flow instability.

Keywords: Thermal viscous fingering, Anisotropic media, Linear stability analysis, Spectral method, Lewis number, Thermal lag.

Introduction

The displacement of liquids through porous media is so important in industrial applications especially in enhanced oil recovery (EOR) (Vafai and Tien, 1981, Whitaker, 1986, Alizadeh, Karimi, Arjmandzadeh and Mehdizadeh, 2019, Yuan, Xu and Zhao, 2020). Among them, fingering instability represent a significant topic of research. The viscous fingering is happened in porous media when a low viscosity liquid displaces a high viscosity one. The difference of viscosity of the two fluids involved in displacements is known to be the key factor associated with this instability. However, the other characteristics of the permeable medium and flow may also affect the severity of this instability. Viscous fingering appears in many environmental, geophysical and industrial processes such as petroleum reservoir engineering (water flooding operations), groundwater filtration, chemical engineering fluidized beds, fixed bed regeneration and so on (Homsy, 1987). In particular, miscible viscous fingering is known to be critical for EOR in geological porous media (Wang and Dong, 2009, Kong, Haghighi and Yortsos, 1992, Berg, Oedai, Landman, Brussee, Boele, Valdez and van Gelder, 2010, Nilsson, Kulkarni, Gerberich, Hammond, Singh, Baumhoff and Rothstein, 2013, Pei, Zhang, Ge, Zhang and Wang, 2014), wherein one fluid is injected to displace another fluid (e.g. crude oil) and the instability reduces the efficiency of this process.

Many analytical, computational and experimental studies have been reported in literature about the viscous fingering instability. The first major contribution in this area is the study of Hill (1952). Subsequently this topic has stimulated considerable attention. Most studies communicated have however focused on isothermal flows through isotropic media. For example, Tan & Homsy (1988) have used the spectral method to numerically simulate the viscous fingering problem. More recently, Shokri, Kayhani, & Norouzi (2017) studied the effect of elasticity on miscible

displacement of non-Newtonian liquids. Yazdi *et al.* (Yazdi and Norouzi, 2018, Norouzi, Yazdi and Birjandi, 2018) have investigated immiscible viscoelastic flows. These studies have identified that the elastic property of viscoelastic fluids can control the fingering instability and successfully increase the displacement efficiency.

Since natural and industrial porous media environments are rarely isotropic, the investigation of flow through anisotropic porous media attracted the attention of some researchers since it more realistically models actual systems. Zimmerman & Homsy (1991) used Hartley transforms to numerically simulate an unstable miscible displacement with anisotropic dispersion. They observed some finger interaction mechanisms which are not present in isotropic dispersion, i.e. multiple coalescence and fading. More recently, Ghesmat and Azaiez (2008) studied the influence of anisotropy of dispersion on the Saffman-Taylor instability. They reported that an anisotropic velocity-dependent tensor has profound effects on the structure of the fingers, the sweep efficiency and the relative contact area of displacements. Norouzi & Shoghi (2014) studied the same problem by considering anisotropic behavior for both permeability and dispersion. They showed that the flow is stabilized by increasing the permeability ratio and decreasing the dispersion ratio of anisotropic porous media. Henderson and Pena (2017) modeled the immiscible water-oil displacement through the anisotropic and heterogeneous domain. They used a multi-parameter equation to model the anisotropy of heterogeneous water-flooded petroleum reservoirs. Their results showed that in some configurations, the anisotropy could stabilize the flow field which is assistive in EOR via water flooding technique. Shokri, Kayhani, & Norouzi. (2018) simulated viscoelastic fingering instability in anisotropic media with a Hartley transform and linear stability analysis (LSA), highlighting the influence of medium anisotropic characteristics on the fingering instability.

In all the afore-mentioned studies, the flow has been assumed to be isothermal, i.e. the displacing and displaced fluids have the same temperature and their viscosity is only depended on the concentration. In some practical petroleum operations such as hot water and steam flooding (Islam and Azaiez, 2010), the fingering instability appears in non-isothermal flows. This instability is termed thermo-viscous fingering instability and the material modulus (especially the viscosity) is depended on both concentration and temperature. In this instability, two fronts appear: the thermal front and the concentration front. The difference between the location and shape of these fronts is arisen from the difference of heat and mass transfer mechanisms in porous media.

Saghir, Chaalal, & Islam (2000) investigated the non-linear double diffusive convection, both numerically (via a finite element technique) and experimentally. Sheorey and Muralidhar (2003) numerically investigated the displacement of heavy crude oil by pressurized hot water through porous media. Their results indicated that the oil recovery process is reliably improved for non-isothermal injection. Pritchard (2004) described a stability analysis to investigate Saffman-Taylor instabilities of two-front (compositional and thermal fronts) systems, emphasizing that instabilities on the compositional front dominate due to the large ratio of thermal to mass diffusion. Moreover, Pritchard (2009) investigated the fingering instability for the scenario in which the viscosity at the front is changed by two factors that diffuse with different rates in his another study. Isalam and Azaiez (2010a, 2010b) investigated the thermo-viscous fingering using both LSA and CFD simulation. In these studies, the effect of mobility ratio and Lewis number have been studied in detail. Mishra, Trevelyan, Almarcha, & De Wit (2010) studied the differential diffusion of solutions on fingering instability. Islam and Azaiez (2011) modeled the thermal viscous fingering in a radial geometry. They showed that the flow in radial geometry has some obvious deviations from the rectilinear geometry which is mostly related to the difference in velocity gradients. Azaiez

and Sajjadi (2012) investigated the stability of two-component displacements in a homogeneous porous media, noting that the different convection speeds of the component fronts significantly alter the instability characteristics. Sajjadi and Azaiez (2013) further studied the non-isothermal displacement. They showed that by increasing the thermal diffusion rate in liquid phase, the lag between the fronts is decreased. Norouzi, Dorrani, Shokri and Beg (2018) investigated the effect of viscous dissipation on this instability, showing that increasing this parameter could stabilize the flow field. Recently, Shabouei and Nakshatrala (2020) considered double-diffusive effects on the miscible displacement. In their research, the limitations of popular formulations used in viscous fingering study with double-diffusive effects are investigated.

As elaborated earlier, most of previous works are limited to isotropic media. Motivated by providing a deeper insight into the characteristics of real porous media (which are typically anisotropic), in the present study, thermal viscous fingering of miscible flows through anisotropic porous media is investigated theoretically. Both linear stability analysis (LSA) and computational fluid dynamics (CFD) simulations are presented. Nonlinear simulations are carried out via a spectral method. The effects of different characteristics of the flow and media on the instability are studied in detail.

MODELING

Problem Statement

In this paper, a horizontal flow through an anisotropic porous medium is studied. A schematic shape of the problem is illustrated in **Figure 1**. The displacing liquid is entered to the domain with a constant velocity and sweep the displaced one. Here, the subscribes 1 and 2 denote the displacing

and displaced liquids, respectively. Since the porous media is anisotropic, both on- and off-axis coordinates are deployed to simulate the permeability and dispersion characteristics of the anisotropic media. Here, $\boldsymbol{K}$ and $\boldsymbol{D}$ are the dispersion and permeability of the domain. For anisotropic domains, $\boldsymbol{K}$ and $\boldsymbol{D}$ are usually measured along on-axis. The on-axis is the principle direction where non-diagonal components of $\boldsymbol{K}$ and $\boldsymbol{D}$ are zero. A coordinate system for any observer can be considered as an off-axis. In this paper, the illustrated *x*- and *y*-axis in Fig. 1 (the main flow and lateral directions) is the off-axis. It is supposed that we can reach from off-axis to on-axis by rotation with angle $-\beta$ around *z* direction. The Darcy law is employed to model the fluid flow and is valid for viscous-dominated scenarios at low Reynolds number. This law in on- and off-axis coordinates can be expressed as:

$$\begin{Bmatrix} q_{x1} \\ q_{x2} \end{Bmatrix}_{on} = -\frac{1}{\eta}\begin{bmatrix} \bar{K}_{11} & 0 \\ 0 & \bar{K}_{22} \end{bmatrix}_{on} \begin{Bmatrix} \dfrac{\partial p}{\partial x_1} \\ \dfrac{\partial p}{\partial x_2} \end{Bmatrix}_{on} \tag{1}$$

$$\begin{Bmatrix} q_{x} \\ q_{y} \end{Bmatrix}_{off} = -\frac{1}{\eta}\begin{bmatrix} K_{11} & K_{12} \\ K_{21} & K_{22} \end{bmatrix}_{off} \begin{Bmatrix} \dfrac{\partial p}{\partial x} \\ \dfrac{\partial p}{\partial y} \end{Bmatrix}_{off} \tag{2}$$

where q is the flow flux, η is viscosity, p is pressure and $\bar{K}_{i,j}$ and $K_{i,j}$ are components of permeability coefficient tensors in the on-axis and off –axis, respectively. The rotation tensor is introduced as:

$$\left[T\left(\beta\right)\right] = \begin{bmatrix} \cos\beta & -\sin\beta \\ \sin\beta & \cos\beta \end{bmatrix} \tag{3}$$

It follows that Eqn. (1) can be rewritten as:

$$\left[T\left(-\beta\right)\right]\boldsymbol{q}_{off} = -\frac{1}{\eta}\boldsymbol{K}_{0n}\left[T\left(-\beta\right)\right]\nabla p_{off} \tag{4}$$

Equation (4) may further be rewritten as:

$$\boldsymbol{q}_{off} = -\frac{1}{\eta}\left[T\left(-\beta\right)\right]^{-1}\boldsymbol{K}_{0n}\left[T\left(-\beta\right)\right]\nabla p_{off} \tag{5}$$

Comparing equations (5) and (2), Eqn. (6) can be deduced:

$$\boldsymbol{K}_{off} = \left[T\left(-\beta\right)\right]^{-1}\boldsymbol{K}_{on}\left[T\left(-\beta\right)\right] \tag{6}$$

For convenience, in following, the off and on subscript used to show the off- and on- axis are omitted.

Based on Eqns. (3) to (6), we have:

$$\begin{bmatrix} K_{11} & K_{12} \\ K_{21} & K_{22} \end{bmatrix} = \begin{bmatrix} \bar{K}_{11}\cos^2\beta_K + \bar{K}_{22}\sin^2\beta_K & \left(\bar{K}_{11} - \bar{K}_{22}\right)\sin\beta_K\cos\beta_K \\ \left(\bar{K}_{11} - \bar{K}_{22}\right)\sin\beta_K\cos\beta_K & \bar{K}_{11}\sin^2\beta_K + \bar{K}_{22}\cos^2\beta_K \end{bmatrix} \tag{7}$$

The same equation can be derived for diffusion as follows:

$$\begin{bmatrix} D_{11} & D_{12} \\ D_{21} & D_{22} \end{bmatrix} = \begin{bmatrix} \bar{D}_{11}\cos^2\beta_D + \bar{D}_{22}\sin^2\beta_D & \left(\bar{D}_{11} - \bar{D}_{22}\right)\sin\beta_D\cos\beta_D \\ \left(\bar{D}_{11} - \bar{D}_{22}\right)\sin\beta_D\cos\beta_D & \bar{D}_{11}\sin^2\beta_D + \bar{D}_{22}\cos^2\beta_D \end{bmatrix} \tag{8}$$

Governing equations

The governing equations consist of the continuity, Darcy's law, and heat and mass transfer equations:

$$\nabla\cdot\boldsymbol{u} = 0 \tag{9}$$

$$\boldsymbol{u} = -\frac{1}{\eta}\boldsymbol{K}\nabla p \tag{10}$$

$$\phi\frac{\partial c}{\partial t} + \boldsymbol{u}.\nabla c = \phi \boldsymbol{D}_C \nabla^2 c \tag{11}$$

$$\phi\frac{\partial T}{\partial t} + \lambda\left(\boldsymbol{u}.\nabla T\right) = \phi \boldsymbol{D}_T \nabla^2 T \tag{12}$$

where $\boldsymbol{u}$ is velocity vector, p is pressure, η is viscosity, $\boldsymbol{K}$ is permeability, ϕ is porosity, c is the concentration, $\boldsymbol{D}_C$ is dispersion, T is temperature and $\boldsymbol{D}_T$ is the heat diffusion. The parameter λ is the ratio of the advancement rate of the temperature field to the concentration field. It is designated as the thermal-lag coefficient and defined as:

$$\lambda = \frac{\phi\rho_f C_{p_f}}{\phi\rho_f C_{p_f} + (1-\phi)\rho_s C_{ps}} \tag{13}$$

where ρ is the density and C_p is the specific heat capacity. Here, the subscripts *f* and *s* denote to the fluid and solid phases.

Boundary conditions and initial conditions

In this study, the following boundary conditions are considered:

$$u\left(x=0,y,t\right)=U \quad v\left(x=0,y,t\right)=0 \quad c\left(x=0,y,t\right)=c_1 \quad T\left(x=0,y,t\right)=T_1 \tag{14}$$

$$u\left(x=L,y,t\right)=U \quad v\left(x=L,y,t\right)=0 \quad c\left(x=L,y,t\right)=0 \quad T\left(x=L,y,t\right)=T_2 \tag{15}$$

$$\left(\mathbf{u},c,T\right)\left(x,y=0,t\right)=\left(\mathbf{u},c,T\right)\left(x,y=W,t\right) \tag{16}$$

The initial conditions are prescribed as follows:

$$T(x,y,t=0)=\begin{cases}T_1+f(x,y) & L<L_x\\ T_2+f(x,y) & L\geq L_x\end{cases} \tag{17}$$

$$c(x,y,t=0)=\begin{cases}c_1+f(x,y) & L<L_x\\ c_2+f(x,y) & L\geq L_x\end{cases} \tag{18}$$

where $f(x,y)$ denotes a random function. $L_x=0$, i.e. at the middle of the porous medium.

Scaling

The following dimensionless groups are used in the present study:

$$\begin{aligned}&\boldsymbol{x}^*=\frac{(x-Ut/\phi,y)}{\bar{D}_{C11}\phi/U},\qquad \boldsymbol{u}^*=\frac{(u-U,v)}{U},\qquad t^*=\frac{t}{\bar{D}_{C11}\phi^2/U^2},\\ &c^*=\frac{c}{c_1},\qquad \eta^*=\frac{\eta}{\eta_1},\quad p^*=\frac{p}{\phi\eta_1\bar{D}_{C11}/\bar{K}_{22}},\\ &\boldsymbol{K}^*=\frac{\boldsymbol{K}}{\bar{K}_{22}},\ \boldsymbol{D}^*=\frac{\boldsymbol{D}}{\bar{D}_{C11}}\quad \theta^*=\frac{T-T_2}{T_1-T_2}\end{aligned} \tag{19}$$

Using Eq. (19), the non-dimensional form of Eqn. (9) to (12) can be derived as follows:

$$\nabla.\boldsymbol{u}^*=0 \tag{20}$$

$$\nabla p^*=-\frac{\eta^*}{\boldsymbol{K}^*}(\boldsymbol{u}^*+i) \tag{21}$$

$$\frac{\partial c^*}{\partial t^*}+\boldsymbol{u}^*.\nabla c^*=\nabla.\left(\boldsymbol{D}_C^*\nabla c^*\right) \tag{22}$$

$$\frac{\partial\theta^*}{\partial t^*}+\lambda\boldsymbol{u}^*.\nabla\theta^*+(\lambda-1)\frac{\partial\theta^*}{\partial x^*}=Le\left(\nabla.\left(\boldsymbol{D}_C^*\nabla\theta^*\right)\right) \tag{23}$$

$$\boldsymbol{D}_C^*=\begin{bmatrix}\cos^2\beta_D+\alpha_D\sin^2\beta_D & (1/2)(1-\alpha_D)\sin 2\beta_D\\ (1/2)(1-\alpha_D)\sin 2\beta_D & \sin^2\beta_D+\alpha_D\cos^2\beta_D\end{bmatrix} \tag{24}$$

$$\boldsymbol{K}^{*}=\begin{pmatrix}\alpha_K\cos^2\beta_K+\sin^2\beta_K & (1/2)(\alpha_K-1)\sin 2\beta_K\\ (1/2)(\alpha_K-1)\sin 2\beta_K & \alpha_K\sin^2\beta_K+\cos^2\beta_K\end{pmatrix} \tag{25}$$

where $\alpha_K=\overline{K}_{11}/\overline{K}_{22}$ and $\alpha_D=\overline{D}_{22}/\overline{D}_{11}$ are the permeability and diffusion ratio, respectively. The terms β_K and β_D are also the angle between the off- and on-axis coordinates for permeability and diffusion. $\boldsymbol{D}_T^*$ is assumed to be equal to $Le\times\boldsymbol{D}_C^*$ where Le is the Lewis number. Here, a Lagrangian moving frame with constant velocity of U is used to solve the problem. The following correlations are employed to model the variation of viscosity with concentration and temperature:

$$\eta^{*}=\exp(\beta_C(1-c^{*})+\beta_T(1-\theta^{*})) \tag{26}$$

where β_C and β_T are two constants of above equation of state that should be measured based on viscometric data of any fluid for practical applications. The dimensionless boundary conditions are:

$$\begin{aligned}&u^{*}\left(x^{*}=-\frac{Pe_C}{2}-t^{*},y^{*},t^{*}\right)=1,\quad v^{*}\left(x^{*}=-\frac{Pe_C}{2}-t^{*},y^{*},t^{*}\right)=0,\\ &c^{*}\left(x=-\frac{Pe_C}{2}-t^{*},y^{*},t^{*}\right)=1,\quad \theta^{*}\left(x=-\frac{Pe_C}{2}-t^{*},y^{*},t^{*}\right)=1,\end{aligned} \tag{27}$$

$$\begin{aligned}&u^{*}\left(x^{*}=\frac{Pe_C}{2}-t^{*},y^{*},t^{*}\right)=1,\quad v^{*}\left(x^{*}=\frac{Pe_C}{2}-t^{*},y^{*},t^{*}\right)=0,\\ &c^{*}\left(x^{*}=\frac{Pe_C}{2}-t^{*},y^{*},t^{*}\right)=0,\quad \theta^{*}\left(x^{*}=\frac{Pe_C}{2}-t^{*},y^{*},t^{*}\right)=0,\end{aligned} \tag{28}$$

$$\left(u^{*},c^{*},\theta^{*}\right)\left(x^{*},y^{*}=-\frac{Pe_C}{2A},t^{*}\right)=\left(u^{*},c^{*},\theta^{*}\right)\left(x^{*},y^{*}=\frac{Pe_C}{2A},t^{*}\right) \tag{29}$$

where $Pe_C=UL/\overline{D}_{C11}\phi$ is the Peclét number and $A=L/W$ denotes the aspect ratio. The dimensionless initial conditions can be derived as:

$$\theta^*(x^*, y^*, t^* = 0) = \begin{cases} 1 + \delta \times rand(y) & Pe_C < L_x^* \\ 0 + \delta \times rand(y) & Pe_C \geq L_x^* \end{cases} \tag{30}$$

$$c^*(x^*, y^*, t^* = 0) = \begin{cases} 1 + \delta \times rand(y) \times \exp(-x^{*2} / \sigma^2) & Pe_C < L_x^* \\ 0 + \delta \times rand(y) \times \exp(-x^{*2} / \sigma^2) & Pe_C \geq L_x^* \end{cases} \tag{31}$$

Here, "*rand* " is a random function that generate the values in the range of -1 to 1 and δ and σ are the size and diffusion of the disturbance, respectively. For simplification, the star superscript is removed from the next equations.

Numerical method

We used the stream function (ψ) and vorticity (ω) relationships in 2D Cartesian coordinate systems to simulate the thermal viscous fingering problem:

$$u = \frac{\partial \psi}{\partial y} \quad , \quad v = -\frac{\partial \psi}{\partial x} \tag{32}$$

$$\omega = \frac{\partial v}{\partial x} - \frac{\partial u}{\partial y} = -\left(\frac{\partial^2 \psi}{\partial x^2} + \frac{\partial^2 \psi}{\partial y^2} \right) \tag{33}$$

By applying the curl operation on the Eq. (21) and then using the transformations, the final equations are expressed as follows:

$$\omega = \frac{2}{\alpha_k + 1 + (\alpha_k - 1)\cos(2\beta_k)} \begin{pmatrix} -H_1(\frac{\partial \psi}{\partial x})\left(\beta_c \frac{\partial c}{\partial x} + \beta_t \frac{\partial \theta}{\partial x}\right) - \\ H_2(\frac{\partial \psi}{\partial y} + 1)\left(\beta_c \frac{\partial c}{\partial y} + \beta_t \frac{\partial \theta}{\partial y}\right) + \\ H_3((\frac{\partial \psi}{\partial y} + 1)\left(\beta_c \frac{\partial c}{\partial x} + \beta_t \frac{\partial \theta}{\partial x}\right) + \\ (\frac{\partial \psi}{\partial x})\left(\beta_c \frac{\partial c}{\partial y} + \beta_t \frac{\partial \theta}{\partial y}\right) - 2\frac{\partial^2 \psi}{\partial y \partial x}) + \\ (1-\alpha_k)\cos 2\beta_k (\frac{\partial^2 \psi}{\partial y^2}) \end{pmatrix} \tag{34}$$

$$\frac{\partial c}{\partial t} + \frac{\partial \psi}{\partial y}\frac{\partial c}{\partial x} - \frac{\partial \psi}{\partial x}\frac{\partial c}{\partial y} = A_1 \frac{\partial^2 c}{\partial x^2} + A_2 \frac{\partial^2 c}{\partial y^2} + A_3 \frac{\partial^2 c}{\partial y \partial x} \tag{35}$$

$$\frac{\partial \theta}{\partial t} + \lambda\left(\frac{\partial \psi}{\partial y}\frac{\partial \theta}{\partial x} - \frac{\partial \psi}{\partial x}\frac{\partial \theta}{\partial y}\right) + (\lambda - 1)\frac{\partial \theta}{\partial x} = Le\left(A_1 \frac{\partial^2 \theta}{\partial x^2} + A_2 \frac{\partial^2 \theta}{\partial y^2} + A_3 \frac{\partial^2 \theta}{\partial y \partial x}\right) \tag{36}$$

where

$$H_1 = (\alpha_K \cos^2 \beta_K + \sin^2 \beta_K) \tag{37}$$

$$\mathrm{H}_2 = (\alpha_K \sin^2 \beta_K + \cos^2 \beta_K) \tag{38}$$

$$H_3 = ((1/2)(1-\alpha_K)\sin 2\beta_K) \tag{39}$$

$$A_1 = (\cos^2 \beta_D + \alpha_D \sin^2 \beta_D) \tag{40}$$

$$\mathrm{A}_2 = (\sin^2 \beta_D + \alpha_D \cos^2 \beta_D) \tag{41}$$

$$A_3 = (1-\alpha_D)\sin 2\beta_D \tag{42}$$

This set of equations is solved using a pseudo-spectral method. By applying the modified Hartley transformation, the PDEs become ordinary differential equations. In order to solve the problem via the mentioned method, it needs to use the periodic boundary conditions. Actually, the

concentration and temperature variables are not periodic in the *x*-direction. Following Manickam and Homsy (1993), theses parameters may be divided into two parts at any times; a basic solution and a disturbance component:

$$c(x,y,t)=\bar{c}(x,t)+c'(x,y,t) \tag{43}$$

$$\theta(x,y,t)=\bar{\theta}(x,t)+\theta'(x,y,t) \tag{44}$$

Here, the disturbances decay according to the specified boundaries of the flow domain. The base state profiles are defined as:

$$\bar{c}(x,t)=\frac{1}{2}(1-erf\ (\frac{x}{2\sqrt{t}})) \tag{45}$$

$$\bar{\theta}(x,t)=\frac{1}{2}(1-erf\ (\frac{x-(\lambda-1)t}{2\sqrt{Let}})) \tag{46}$$

Now, we should find the disturbances to determine the total solutions. In this way, periodicity of all boundary conditions is enforced. The time-marching in the parameters is achieved with the popular and stable 4th order Adams-Bashforth method.

LINEAR STABILITY ANALYSIS (LSA)

In order to study the problem via LSA, a basic solution is considered for solving the governing equations as follows:

$$u_0=v_0=0 \tag{47}$$

$$\frac{\partial p_0}{\partial x}=-\frac{H_2}{H_4}\eta_0 \tag{48}$$

$$\frac{\partial c_0}{\partial t} = A_1 \frac{\partial^2 c_0}{\partial x^2} \tag{49}$$

$$\frac{\partial \theta_0}{\partial t} + (\lambda - 1)\frac{\partial \theta_0}{\partial x} = A_1 \frac{\partial^2 \theta_0}{\partial x^2} \tag{50}$$

$$\eta_0 = e^{\beta_C (1-c_0)+\beta_T (1-\theta_0)} \tag{51}$$

In the above equations, H_2 and A_1 are defined by Eqns. (38) and (40), respectively. H_4 is expressed as:

$$H_4 = (\alpha_k \sin^2 \beta_k + \cos^2 \beta_k) * (\alpha_k \cos^2 \beta_k + \sin^2 \beta_k) - (1/4)((\alpha_k - 1)\sin 2\beta_k)^2 \tag{52}$$

By considering disturbances in parameters of problem and subtracting the governing equations that contain the disturbances from the governing equations of basic solution, we have:

$$\frac{\partial u'}{\partial x} + \frac{\partial v'}{\partial y} = 0 \tag{53}$$

$$\frac{\partial p'}{\partial x} + H_2 \left(\frac{\eta_0}{H_4} u' + \frac{\eta'}{H_4}\right) + H_3 \frac{\eta_0}{H_4} v' = 0 \tag{54}$$

$$\frac{\partial p'}{\partial y} + H_3 \left(\frac{\eta_0}{H_4} u' + \frac{\eta'}{H_4}\right) + H_1 \frac{\eta_0}{H_4} v' = 0 \tag{55}$$

$$\frac{\partial c'}{\partial t} + u' \frac{\partial c_0}{\partial x} = A_1 \frac{\partial^2 c'}{\partial x^2} + A_2 \frac{\partial^2 c'}{\partial y^2} + A_3 \frac{\partial^2 c'}{\partial x \partial y} \tag{56}$$

$$\frac{\partial \theta'}{\partial t} + \lambda u' \frac{\partial \theta_0}{\partial x} + (\lambda - 1)\frac{\partial \theta'}{\partial x} = Le\left(A_1 \frac{\partial^2 \theta'}{\partial x^2} + A_2 \frac{\partial^2 \theta'}{\partial y^2} + A_3 \frac{\partial^2 \theta'}{\partial x \partial y}\right) \tag{57}$$

$$\eta' = -\eta_0 \left(R_C c' + R_T \theta'\right) \tag{58}$$

H_{1-4} and A_{1-3} are defined in equations (37-42) and (52).

Combining the Eqns. (53) - (55), the following equation is obtained:

$$H_2\left(\frac{\partial^2 u'}{\partial y^2}+\frac{\partial^2 \eta'}{\eta_0 \partial y^2}\right)+H_3\left(-2\frac{\partial^2 u'}{\partial y\,\partial x}-\frac{\partial u'}{\partial y}\frac{\partial \eta_0}{\eta_0 \partial x}-\frac{\partial^2 \eta'}{\eta_0 \partial x\,\partial y}\right)+H_1\left(\frac{\partial^2 u'}{\partial x^2}+\frac{\partial u'}{\partial x}\frac{\partial \eta_0}{\eta_0 \partial x}\right)=0 \tag{59}$$

We considered the following relationships for unknowns of linearized equations:

$$(c',u',\theta')=(C,U,\theta)(x)e^{\sigma(t_0)t}e^{iky} \tag{60}$$

In Eq. (60), σ and k are the growth rate and wave number of disturbances, respectively. By inserting equation (60) into the linearized equations, we have:

$$\left[H_1\frac{d^2}{dx^2}+\left(\frac{\partial \eta_0}{\eta_0 \partial x}-2ikH_3\right)\frac{d}{dx}+\left(-k^2H_2-ikH_3\frac{\partial \eta_0}{\eta_0 \partial x}\right)\right]U+\left[ik\beta_C H_3\frac{d}{dx}+k^2\beta_C H_2\right]C+\left[ik\beta_T H_3\frac{d}{dx}+k^2\beta_T H_2\right]\theta=0 \tag{61}$$

$$\left[\sigma(t_0)-A_1\frac{d^2}{dx^2}+A_2k^2-A_3ik\frac{d}{dx}\right]C=-U\frac{dc_0}{dx} \tag{62}$$

$$\left[-LeA_1\frac{d^2}{dx^2}+\left((\lambda-1)-A_3Leik\right)\frac{d}{dx}+\sigma(t_0)+A_2Lek^2\right]\theta=-\lambda U\frac{d\theta_0}{dx} \tag{63}$$

RESULTS AND DISCUSSION

Linear stability analysis (LSA)

A sixth order shooting method is employed to solve the eigenvalue system specified by Eqns. (61-63). Here, the largest possible eigenvalues that produced non-zero solution are computed. The numerical domain has been selected to be sufficiently large to determine these eigenvalues. Except some especial cases, the results are presented at $Pe_C=1000$, $A=2$, $Le=1$, $\beta_C=\beta_T=1.5$, $\lambda=0.75$, $t_0=0.1$, $\alpha_D=\alpha_K=1$ and $\beta_D=\beta_K=0$. For verification, the growth rate of

disturbance of a non-isothermal movement through isotropic porous media is depicted in **Figure 2**. The results of present study is illustrated by a continuous line and the results of (Islam and Azaiez, 2010) are shown via a dashed line with squares for $\beta_T = 1$ and circles for $\beta_T = 2$. Here, $Le = \lambda = 1$ and $\beta_C = 1$. Based on the figure, the results of present study have a good agreement with the work of Islam and Azaiez (Islam and Azaiez, 2010). Confidence in the present stability analysis is therefore justifiably high.

In order to investigate the influence of anisotropic parameters of porous media on the thermo-viscous fingering, the variation of the growth rate in terms of the wave number for different parameters of the porous medium is plotted. **Figures 3** and **4** illustrate the growth rate at different anisotropic permeability ratios (α_K) and different anisotropic permeability angles (β_K), respectively. Increasing α_K and decreasing β_K lead to more stable flows. The effects of the dispersion ratio (α_D) and the dispersion angle (β_D) on the stability characteristics are shown in **Figures 5** and **6**, respectively. These parameters exert a stabilizing effect and the growth rates decrease by increasing α_D and β_D.

Numerical simulation

Here, the results of the CFD modeling are presented to show how the different dimensionless parameters characterizing the flow displacement influence the fingering instability. Except some especial cases, the CFD simulations are done at $Pe_C = 1000$, $A = 2$, $Le = 1$ and $\lambda = 0.75$.

Contours of results

In the followings, the concentration and temperature iso-contours (*c* and *T*) were depicted as time sequences. Initially, the instability is started via inserting a fluctuation at interfaces between two

liquids. The finger-like patterns are rapidly created and grown in the domain. As mentioned before, the main factor on fingering instability is a difference between the viscosity of two liquids. The temperature and concentration dependency of viscosity are also adjusted by β_C and β_T (refer to Eq. (26)) and their values may be positive or negative. When higher viscosity fluid is ahead of the front, these parameters are positive and are therefore associated with instability. For negative values of these parameters, the conditions are the opposite. For clarity, the results of this section are ordered in three groups: 1) β_C and $\beta_T > 0$, 2) $\beta_C > 0$ and $\beta_T < 0$ and 3) $\beta_C < 0$ and $\beta_T > 0$.

Positive concentration and temperature mobility ratios

In what follows, a hot liquid with low viscosity sweeps a cold one with higher value of viscosity. This means that we have $\beta_C > 0$ and $\beta_T > 0$. Unless specified otherwise, the problem is simulated for $\beta_C = 1.5$ and $\beta_T = 1.5$. **Figure 7** shows iso-contours of concentration and temperature at $\lambda = 0.75$ and $\lambda = 1$. In this figure, $\alpha_K = 1.8$, $\alpha_D = 0.9$ and $\beta_D = \beta_K = \pi/3$. When the thermal-lag coefficient is less than one, the heat transfer between the body of porous media and the liquids is considerable. So, the speed of progression of the thermal front is declined and as a result, this front lags behind the concentration front. For $\lambda = 1$, there is no heat dissipation and both fronts progress together possessing the same structure. As a result, there is a complete interaction between the two fronts. Since both fronts have a destabilizing effect, it is normal that in the case of complete interaction ($\lambda = 1$), the flow is more unstable. Close inspection of the contours indicates that the coalescence mechanism is recognizable. In this mechanism (which is specified by circulars), path of one of fingers is deviated to the neighboring one and merged together. Another mechanism that existed in this figure is the tip-splitting. Here, one finger is divided into

two fingers (see the case at $t = 300$). **Figure 8** shows the influnce of Lewis number on distributions of concentration and temperature. Here, $\alpha_K = 1.8$, $\alpha_D = 0.9$ and $\beta_D = \beta_K = \pi/3$. Higher Lewis number physically means that the heat diffuses quicker than the species (solute) and the two fronts attain thermal equilibrium faster. For the cases in which the temperature of displacing liquid is more than the temperature of displaced one, the transfer of thermal energy causes a reduction in the viscosity of the displaced liquid (this acts in favor of stability). Therefore, at higher Lewis number, the flow is more stable. Since $\lambda < 1$, the thermal front is weaker than the concentration front. When $Le > 1$, it becomes weaker and its destabilizing effect decreases. It may be inferred that there is a wavy thermal front instead of a fingering thermal front.

Figure 9 depicts the effect of α_K on the thermo-viscous fingering. The other parameters are considered as $\alpha_D = 1$ and $\beta_K = \beta_D = 0$. The ratio of the permeability along the longitudinal direction to the permeability along the transverse direction is named as α_K. In order to achieve finger growth, the primary disturbances should diffuse in perpendicular to the fluid flow direction. Therefore, at higher values of α_K, the favorable conditions for growing fingers become limited. It can be seen that the fingers on both fronts for $\alpha_K = 2.4$ are smaller than $\alpha_K = 1.2$. The iso-contours of the flow displacements for $\alpha_K = 1$, $\beta_K = \beta_D = 0$ and two values of α_D (i.e. 0.3 and 0.7) are depicted in **Figure 10.** The dispersion ratio is defined as dispersion in the lateral direction to that in the longitudinal one. In this figure, a large number of fingers is witnessed. The transversal dispersion equalizes the fronts of the fingers. At low values of this parameter, the hydrodynamic mechanisms of spreading and shielding have been weakened. In the spreading mechanism, the fingers are formed so that their width is increased and their number is reduced. In the shielding mechanism, some fingers shield the development of the nearby fingers and joint together to

procedure a bigger finger. Therefore, at lower values of α_D, the number of fingers is higher. An interesting phenomenon which is observed relates to the anchoring of the tip of the finger in the case of $\alpha_D = 0.3$. This is shown via a square for $t = 600$. At $\alpha_D = 0.7$, there is a more intensified interaction of fingers in the transverse direction than for $\alpha_D = 0.3$. Therefore, at the last time of simulation, few numbers of fingers with more width can be seen in contours. It can be concluded that the flow is stabilized by increasing α_D.

Figure 11 illustrated the influence of permeability angle β_K on the thermo-viscous fingering contours. As β_K increases, the permeability in the longitudinal direction (K_{11}) decreases whereas the permeability in the transverse direction (K_{22}) increases. As mentioned before, the reduction in the longitudinal permeability and elevation in transverse permeability results in a more unstable flow. Therefore, it follows that the flow through the porous medium with $\beta_K = \pi/6$ is more stable than that for $\beta_K = \pi/3$. Having a close look at the contours reveals that the fingers are smaller at lower values of β_K.

Positive concentration ratio and negative temperature mobility ratio

For $\beta_C > 0$ and $\beta_T < 0$, a liquid with lower temperature and viscosity sweeps a hot liquid with higher viscosity. In this condition, the temperature gradient stabilizes the flow field but concentration gradient has a reverse effect and intensify the hydrodynamic instability. Unless specified otherwise, the results are presented for $\beta_C = 3$ and $\beta_T = -1.5$. **Figure 12** shows the influence of λ on a flow displacement with $\beta_C > 0$ and $\beta_T < 0$. Here, $\alpha_K = 1.8$, $\alpha_D = 0.9$ and

$\beta_D = \beta_K = \pi/3$. The flow is stabilized by growing λ, which could be attributed to the stronger interactions between two fronts and increasing the positive influence of temperature gradient on the flow stability.

Figure 13 shows the iso-contours for two Lewis numbers at $\beta_C > 0$ and $\beta_T < 0$. The other parameters are $\alpha_K = 1.8$, $\alpha_D = 0.9$ and $\beta_D = \beta_K = \pi/3$. Here, higher Le means the displacing liquid cools the warmer displaced liquid faster. Therefore, the viscosity of displaced liquid increases and the factor of instability becomes stronger. As a result, the flow is destabilized by growing Le in these conditions and the thermal front morphs into a strong wavy shape, instead of the form of discrete weak narrow fingers. The iso-contours of *c* and *T* are shown in **Figure 14** for $\alpha_K = 1.2$ and $\alpha_K = 2.4$ where $\alpha_D = 1$ and $\beta_K = \beta_D = 0$. Similar to the previous case (i.e. positive concentration and temperature mobility ratios), α_K does not have much effect on the structure of the fingers. However, it is also apparent in this case that the fingers seem to be shortened by increasing α_K. The effect of α_D on the thermo-viscous fingering is shown in **Figure 15**. Here, $\alpha_K = 1$ and $\beta_K = \beta_D = 0$. For this scenario, the number of fingers is very high and in fact exceeds the number computed in **Figure 10** which has same porous medium properties. The fingers are narrower for lower α_D and it is seen the flow is stabilized by growing this parameter.

Negative concentration mobility ratio and positive temperature mobility ratio

Here, a liquid with high temperature and viscosity sweeps a cold liquid with lower viscosity. In the absence of temperature gradients, this displacement is stable. However, temperature gradients have a destabilizing effect on flow. Unless specified otherwise, the concentration mobility ratio and temperature mobility ratio are fixed as $\beta_C = -1.5$ and $\beta_T = 3$. For these

conditions, in **Figure 16**, the flow displacements with $\lambda = 0.75$ and $\lambda = 0.85$ are compared with one other. The parameters of the porous medium are prescribed as $\alpha_K = 1.8$, $\alpha_D = 0.9$ and $\beta_D = \beta_K = \pi/3$. Unlike the former scenarios, some backward fingers are created in the concentration distribution. Additionality, increasing λ leads to a more unstable flow. As mentioned, temperature gradients have a destabilizing effect on flow. Therefore, as the temperature front is closer to the concentration front (higher λ), the temperature gradient instability impacts more strongly the concentration front. At $\lambda = 0.75$ and $t = 600$, the tip-splitting mechanism can be seen for concentration front. Then, two new branching-fingers bend towards their adjacent fingers and finally merge into their body. In other words, the coalescence mechanism follows the tip-splitting mechanism. With increasing instability, the fingers interaction mechanisms are observed in the concentration front. The coalescence mechanism was shown via squares for $t = 700$.

Figure 17 depicts the contours of *c* and *T* at $Le = 1$ and $Le = 5$. Here, $\alpha_K = 1.8$, $\alpha_D = 0.9$ and $\beta_D = \beta_K = \pi/3$. In the case of $Le = 5$, there are no major fingers in the concentration and temperature contours. Indeed, heat transfer between liquids leads to a depletion in the viscosity of the displaced fluid. Therefore, the flow becomes more stable at higher Le, owing to the enhanced heat transfer. At high Lewis numbers, the destabilizing effect of temperature gradients is significantlyweakened.

Figure 18. depicts the influence of α_K on the *c* and *T* for two different values of 1.2 and 2.4. The other parameters of porous medium are $\alpha_D = 1$ and $\beta_K = \beta_D = 0$. Here, by increasing α_K , the

fingers tend to advance in a straight line, i.e. they grow in the path with higher permeability and the bending of fingers is minimized.

Figure 19 shows the effect of α_D on displacements with $\beta_C < 0$ and $\beta_T > 0$ through a porous medium with $\alpha_K = 1$ and $\beta_K = \beta_D = 0$. As in the earlier cases analyzed, the intensity of instability is reduced by increasing α_D. Here, the interesting point is appearance of tip-splitting mechanism in contours of concentration. This was shown via a circle at $t = 800$. Based on the figure, the intensity of instability is high in the case of $\alpha_D = 0.3$.

Transversely-Averaged Profiles

Examining flow characteristic profiles averaged over one dimension is a common tool in the study of unstable miscible displacements. In this section, the transversely-averaged diagrams of *c* and *T* were reported. **Figure 20** shows the influence of λ on the *c* and *T* averaged profiles. Here, $\alpha_K = 1.8$, $\alpha_D = 0.9$, $\beta_D = \beta_K = \pi/3$ and $t = 450$. The profiles are marked by C and θ related to the averaged concentration and temperature, respectively. As λ decreases, the front of *T* marches with increasingly delay behind of the front of *c*. This is due to the decreasing the velocity of the thermal diffusion ($U_T = \lambda U$) and increasing the heat transfer between the solid and fluids phases. Based on the **Figure 20a**, the concentration gradients intensify the instability, whereas the temperature gradients exert a stabilizing effect at $\beta_C = 3$ and $\beta_T = -1.5$. Therefore, when the two fronts are closer, the flow is more stable and the intensity of peaks in the unstable concentration profiles decreases. The conditions

for **Figure 20b** are opposite, i.e. $\beta_C = -1.5$ and $\beta_T = 3$. Here, the temperature gradients have a destabilizing effect. Therefore, the peaks appear on the temperature averaged profiles. For $\beta_C = \beta_T = 1.5$, both factors have a destabilizing effect. Therefore, more peaks are created when they match each other ($\lambda = 1$) and when they are away from each other, the intensity of instability decreases.

Mixing length

Another useful tool to characterize and quantify the mixing zone is the mixing length. It is defined as the distance of the zone where the transversely-averaged concentration changes from 0.99 to 0.01. **Figure 21** shows the history of mixing length for different λ and three cases: (a) $\beta_C = 3$ and $\beta_T = -1.5$,(b). $\beta_C = -1.5$ and $\beta_T = 3$, and (c) $\beta_C = \beta_T = 1.5$. Here, as with **Figure 20**, $\alpha_K = 1.8$, $\alpha_D = 0.9$, $\beta_D = \beta_K = \pi/3$. In cases (b) and (c), the temperature gradients intensify the fingering instability. Therefore, the thermal front progresses faster and the flow becomes more unstable. Hence, the mixing length increases by growing λ in these cases. However, when β_T is negative, such as in case (a), λ acts to stabilize the flow and the mixing length decreases by growing this parameter. The influence of *Le* on the mixing length is shown in **Figure 22.** Here, $\alpha_K = 1.8$, $\alpha_D = 0.9$, $\beta_D = \beta_K = \pi/3$ and $\lambda = 0.85$. By growing *Le*, the effect of β_T on the flow decreases. Therefore, when β_T is negative and it has a stabilizing effect, the higher Lewis number leads to a more unstable flow. Therefore, in case (a), the mixing length is reduced by growing Le and in cases (b) and (c), the opposed trend is seen. **Figure 23** depicts the influence of the permeability ratio (α_K) for $\alpha_D = 1$, $\beta_K = \beta_D = 0$. Based on the results, the mixing length is

reduced by growing α_K for all cases. As mentioned, increasing the permeability in the longitudinal direction acts in favor of stability. When comparing the results for different β_K in **Figure 24**, it becomes clear that the intensity of instability is increased by growing β_K and the flow regime exhibits a higher mixing length at higher β_K in all cases.

Sweep efficiency

In fingering instability analysis, it is important to quantify how effective the displacement is and how different the fluid and porous media parameters influence the displacement. For example, in enhanced oil recovery, an important consideration is that the injected fluid could extract a larger amount of oil of the reservoir and therefore a means of measuring this ability is essential. This is termed the sweep efficiency. In petroleum engineering, this is defined as the percentage of a well which is swept via an injected liquid. In numerical simulations, following Ghesmat and Azaiez (Ghesmat and Azaiez, 2008), the sweep efficiency is calculated as the ratio of amount of grids with $c \geq 0.5$ to the amount of grids placed behind the front. In **Figure 25**, the effect of λ on the sweep efficiency is shown. Here, $\alpha_K = 1.8$, $\alpha_D = 0.9$, $\beta_D = \beta_K = \pi/3$. As expected and in consistency with the earlier results, when β_T is negative (case a), λ has a stabilizing effect and the sweep efficiency increases by increasing λ. However, when $\beta_T > 0$ (cases b and c), increasing λ leads to a reduction in the sweep efficiency. **Figure 26** depicts the diagrams of sweep efficiency versus the dimensionless time for different values of *Le*. Here, $\alpha_K = 1.8$, $\alpha_D = 0.9$, $\beta_D = \beta_K = \pi/3$ and $\lambda = 0.85$. It can be seen that increasing Le causes a reduction in the sweep efficiency for case (a) and increasing sweep efficiency for cases (b) and (c). For case (b), the sweep

efficiency is close to one, especially at higher Le . This is due to the uniform progression of the concentration front. In **Figures 27** and **28**, the sweep efficiency is displayed as a function of α_D and β_D , respectively. In general, increasing these parameters leads to increasing the sweep efficiency. However, it is evident that in the presence of stabilizing gradients, the effect of β_D on the sweep efficiency is too weak.

Conclusions

In this paper, the effect of anisotropy of porous media on thermal viscous fingering instability been investigated via both LSA and CFD approaches. The principal results have shown that:

(i) When β_T is negative and temperature gradients act to stabilize the flow, increasing Le leads to a more stable flow.

(ii)When β_T is positive and temperature gradients have a destabilizing effect, Le act to destabilize the flow.

(iii) For λ (thermal-lag coefficient), the trend is completely opposite to that computed for the influence of Le .

(iv) In all cases, the flow is stabilized by increasing α_K , α_D and β_D and decreasing β_K . This implies that the longitudinal direction permeability and the transverse direction dispersion exert a significant controlling effect on the thermal viscous fingering instability.

Data Availability Statement

All data, models and code that support the findings of this study are available from the corresponding author upon reasonable request.

References

Alizadeh, R., Karimi, N., Arjmandzadeh, R., & Mehdizadeh, A. (2019). Mixed convection and thermodynamic irreversibilities in MHD nanofluid stagnation-point flows over a cylinder embedded in porous media. *Journal of Thermal Analysis and Calorimetry, 135*(1), 489-506.

Azaiez, J., & Sajjadi, M. (2012). Stability of double-diffusive double-convective miscible displacements in porous media. *Physical Review E, 85*(2), 026306.

Berg, S., Oedai, S., Landman, A., Brussee, N., Boele, M., Valdez, R., & van Gelder, K. (2010). Miscible displacement of oils by carbon disulfide in porous media: Experiments and analysis. *Physics of Fluids, 22*(11), 113102.

Ghesmat, K., & Azaiez, J. (2008). Viscous fingering instability in porous media: effect of anisotropic velocity-dependent dispersion tensor. *Transport in Porous Media, 73*(3), 297-318.

Henderson, N., & Pena, L. (2017). Simulating effects of the permeability anisotropy on the formation of viscous fingers during waterflood operations. *Journal of Petroleum Science and Engineering, 153*, 178-186.

Hill, S. (1952). Channeling in packed columns. *Chemical Engineering Science, 1*(6), 247-253.

Homsy, G. M. (1987). Viscous fingering in porous media. *Annual review of fluid mechanics, 19*(1), 271-311.

Islam, M., & Azaiez, J. (2010a). Miscible thermo-viscous fingering instability in porous media. Part 1: Linear stability analysis. *Transport in Porous Media, 84*(3), 821-844.

Islam, M., & Azaiez, J. (2010b). Miscible thermo-viscous fingering instability in porous media. Part 2: Numerical simulations. *Transport in Porous Media, 84*(3), 845-861.

Islam, M., & Azaiez, J. (2011). Thermo-viscous fingering in quarter five-spot miscible displacements. *European Journal of Mechanics-B/Fluids, 30*(1), 107-119.

Kong, X., Haghighi, M., & Yortsos, Y. (1992). Visualization of steam displacement of heavy oils in a Hele-Shaw cell. *Fuel, 71*(12), 1465-1471.

Manickam, O., & Homsy, G. (1993). Stability of miscible displacements in porous media with nonmonotonic viscosity profiles. *Physics of Fluids A: Fluid Dynamics, 5*(6), 1356-1367.

Mishra, M., Trevelyan, P., Almarcha, C., & De Wit, A. (2010). Influence of double diffusive effects on miscible viscous fingering. *Physical review letters, 105*(20), 204501.

Nilsson, M. A., Kulkarni, R., Gerberich, L., Hammond, R., Singh, R., Baumhoff, E., & Rothstein, J. P. (2013). Effect of fluid rheology on enhanced oil recovery in a microfluidic sandstone device. *Journal of Non-Newtonian Fluid Mechanics, 202*, 112-119.

Norouzi, M., Dorrani, S., Shokri, H., & Beg, O. (2018). Effects of viscous dissipation on miscible thermo-viscous fingering instability in porous media. *International Journal of Heat and Mass Transfer*.

Norouzi, M., & Shoghi, M. (2014). A numerical study on miscible viscous fingering instability in anisotropic porous media. *Physics of Fluids, 26*(8), 084102.

Norouzi, M., Yazdi, A., & Birjandi, A. (2018). A numerical study on Saffman-Taylor instability of immiscible viscoelastic-Newtonian displacement in a Hele-Shaw cell. *Journal of Non-Newtonian Fluid Mechanics, 260*, 109-119.

Pei, H., Zhang, G., Ge, J., Zhang, L., & Wang, H. (2014). Effect of polymer on the interaction of alkali with heavy oil and its use in improving oil recovery. *Colloids and Surfaces A: Physicochemical and Engineering Aspects, 446*, 57-64.

Pritchard, D. (2004). The instability of thermal and fluid fronts during radial injection in a porous medium. *Journal of Fluid Mechanics, 508*, 133-163.

Pritchard, D. (2009). The linear stability of double-diffusive miscible rectilinear displacements in a Hele-Shaw cell. *European Journal of Mechanics-B/Fluids, 28*(4), 564-577.

Saghir, M., Chaalal, O., & Islam, M. (2000). Numerical and experimental modeling of viscous fingering during liquid–liquid miscible displacement. *Journal of Petroleum Science and Engineering, 26*(1-4), 253-262.

Sajjadi, M., & Azaiez, J. (2013). Dynamics of fluid flow and heat transfer in homogeneous porous media. *The Canadian Journal of Chemical Engineering, 91*(4), 687-697.

Shabouei, M., & Nakshatrala, K. (2020). On numerical stabilization in modeling double-diffusive viscous fingering. *Transport in Porous Media, 132*(1), 39-52.

Sheorey, T., & Muralidhar, K. (2003). Isothermal and non-isothermal oil–water flow and viscous fingering in a porous medium. *International journal of thermal sciences, 42*(7), 665-676.

Shokri, H., Kayhani, M., & Norouzi, M. (2017). Nonlinear simulation and linear stability analysis of viscous fingering instability of viscoelastic liquids. *Physics of Fluids, 29*(3), 033101.

Shokri, H., Kayhani, M., & Norouzi, M. (2018). Saffman–Taylor instability of viscoelastic fluids in anisotropic porous media. *International Journal of Mechanical Sciences, 135*, 1-13.

Tan, C., & Homsy, G. (1988). Simulation of nonlinear viscous fingering in miscible displacement. *The Physics of fluids, 31*(6), 1330-1338.

Vafai, K., & Tien, C. L. (1981). Boundary and inertia effects on flow and heat transfer in porous media. *International Journal of Heat and Mass Transfer, 24*(2), 195-203.

Wang, J., & Dong, M. (2009). Optimum effective viscosity of polymer solution for improving heavy oil recovery. *Journal of Petroleum Science and Engineering, 67*(3-4), 155-158.

Whitaker, S. (1986). Flow in porous media I: A theoretical derivation of Darcy's law. *Transport in Porous Media, 1*(1), 3-25.

Yazdi, A. A., & Norouzi, M. (2018). Numerical study of Saffman–Taylor instability in immiscible nonlinear viscoelastic flows. *Rheologica Acta, 57*(8-9), 575-589.

Yuan, Y., Xu, K., & Zhao, K. (2020). Numerical analysis of transport in porous media to reduce aerodynamic noise past a circular cylinder by application of porous foam. *Journal of Thermal Analysis and Calorimetry, 141*(5), 1635-1646.

Zimmerman, W., & Homsy, G. (1991). Nonlinear viscous fingering in miscible displacement with anisotropic dispersion. *Physics of Fluids A: Fluid Dynamics, 3*(8), 1859-1872.

FIGURES

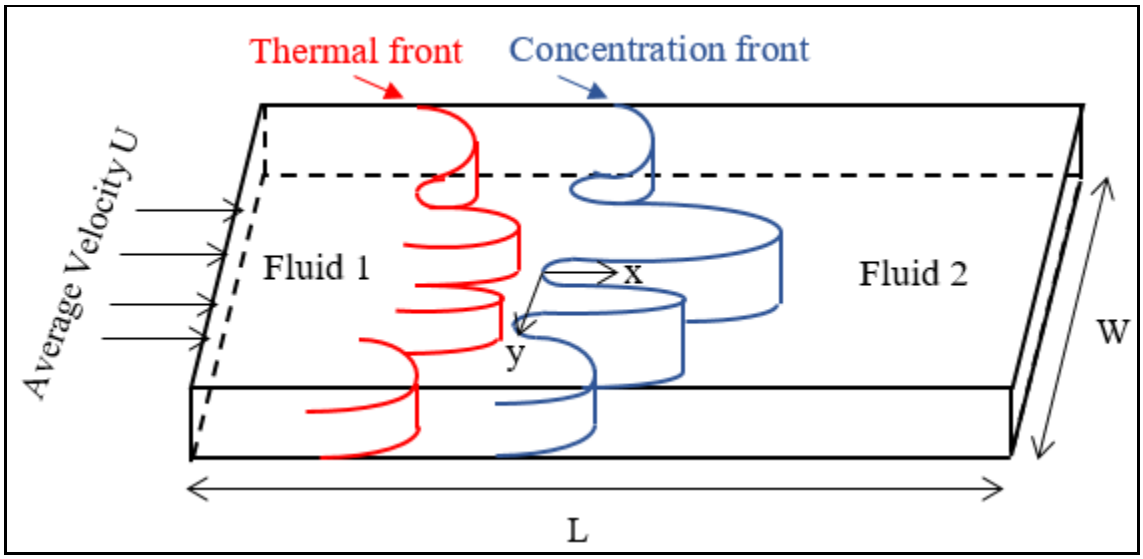

Fig.1. Schematic of the problem.

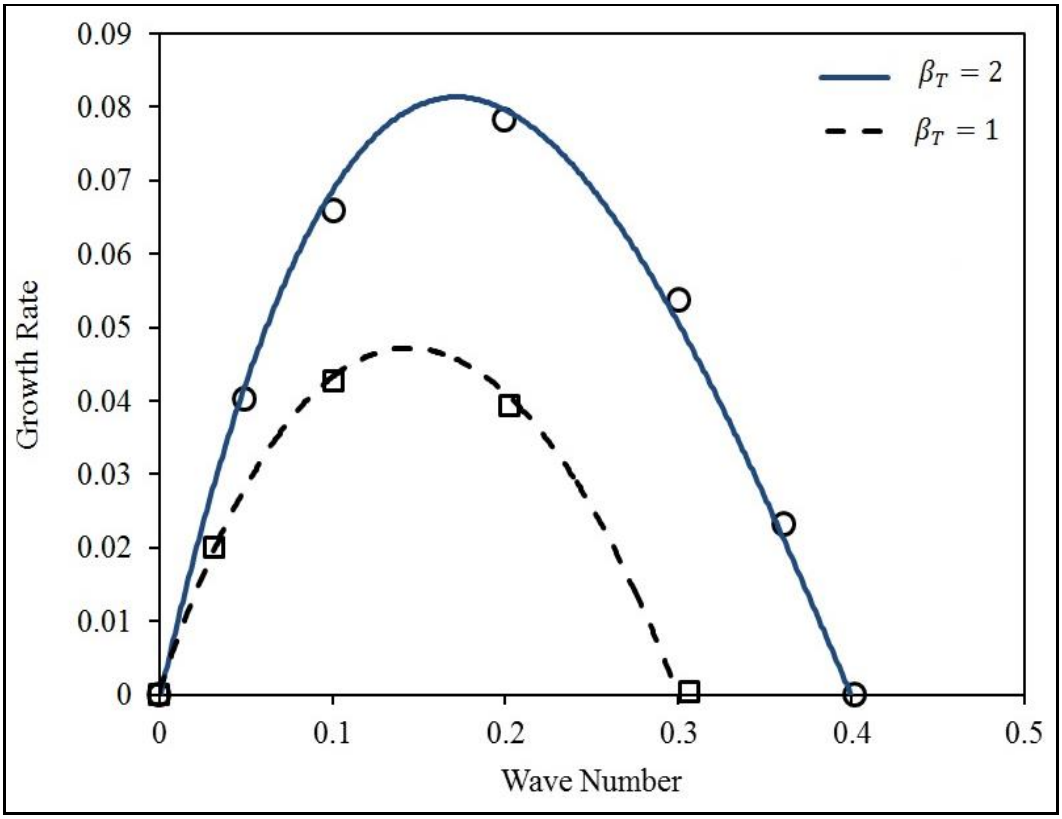

Fig. 2. Instability characteristics for non-isothermal viscous fingering instability: comparison between the results of the present study and those of Islam and Azaiez (2010a).

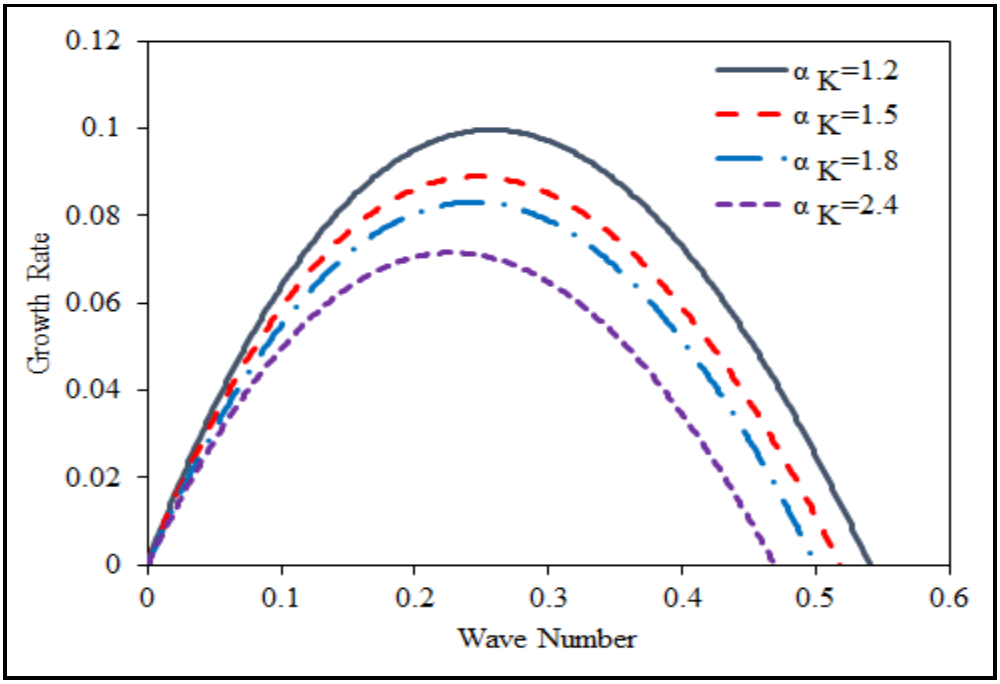

Fig. 3. Instability characteristics for different anisotropic permeability ratios (α_K).

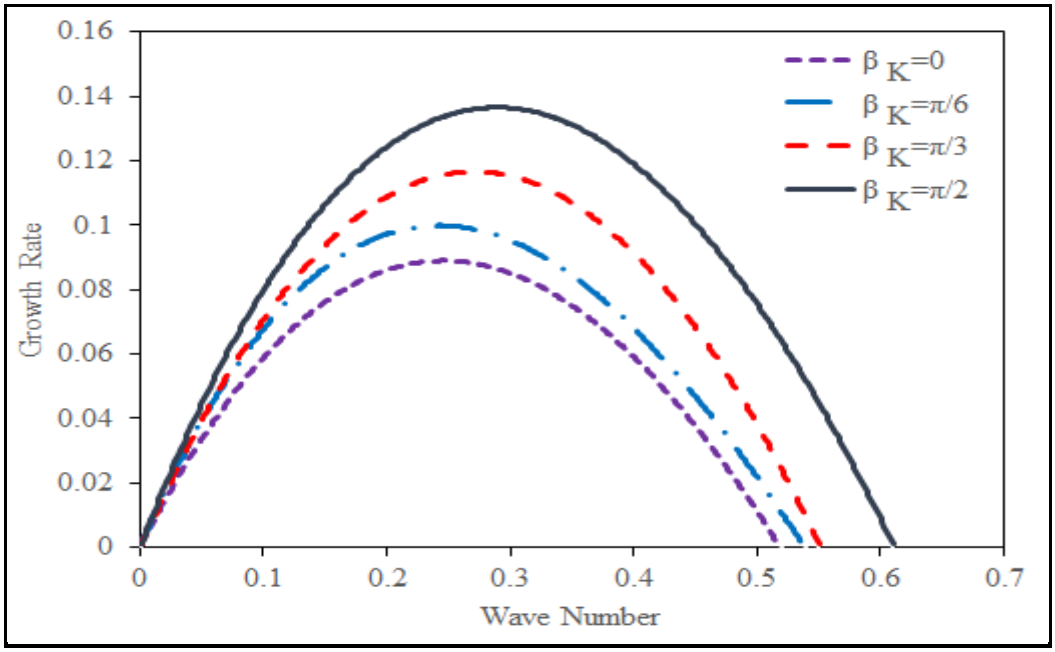

Fig. 4. Instability characteristics for different anisotropic permeability angles (β_K).

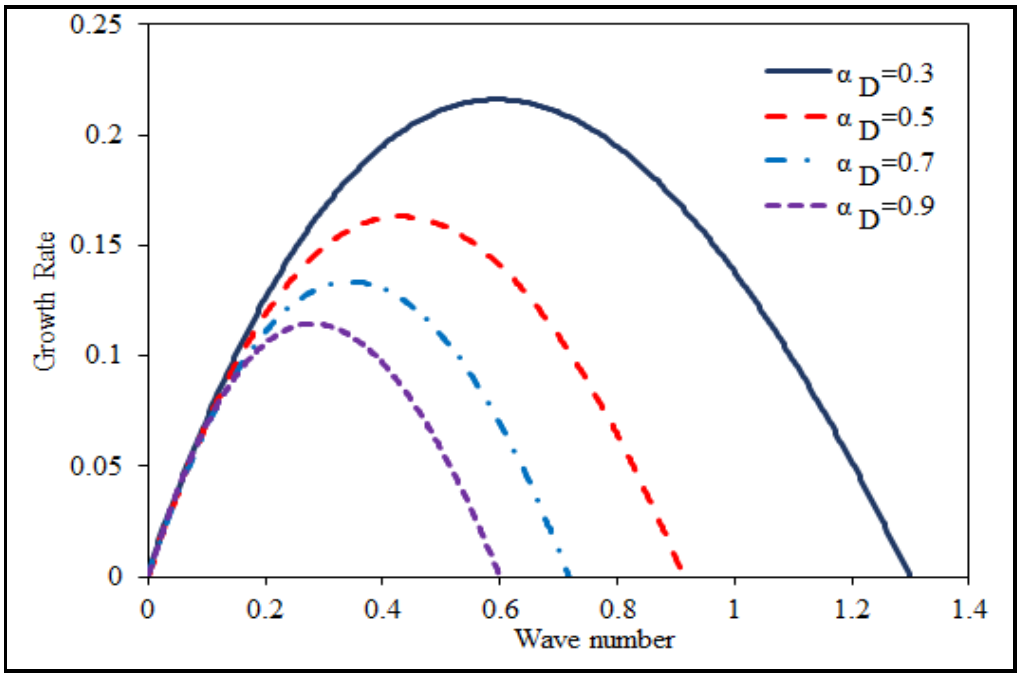

Fig. 5. Instability characteristics for different anisotropic dispersion ratios (α_D).

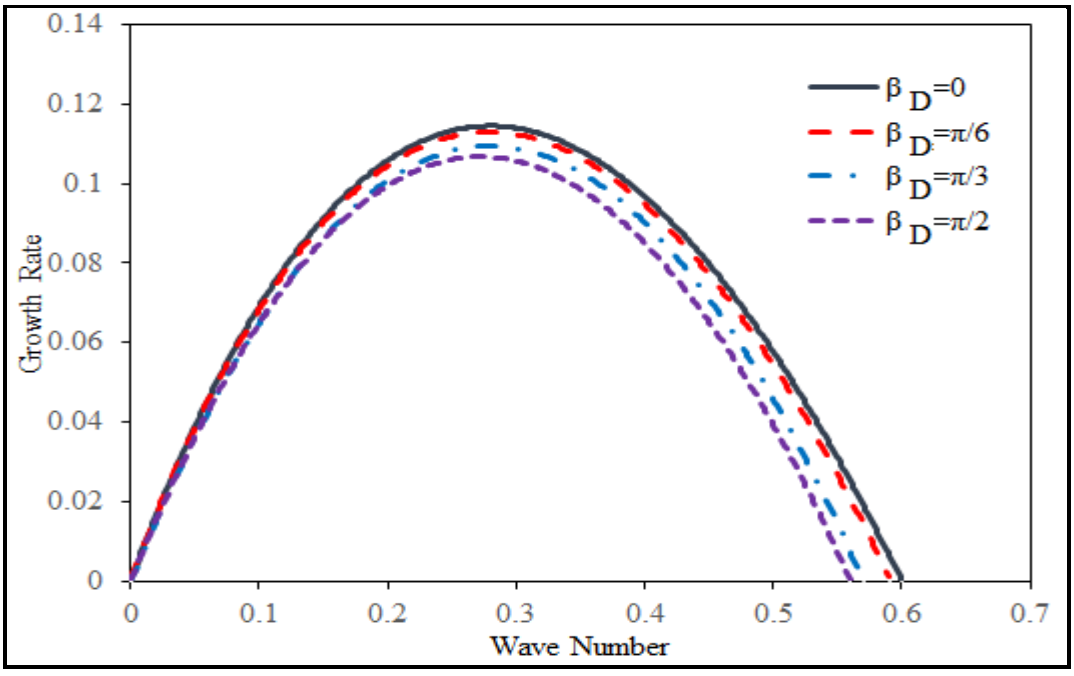

Fig. 6. Instability characteristics for different anisotropic dispersion angles (β_D).

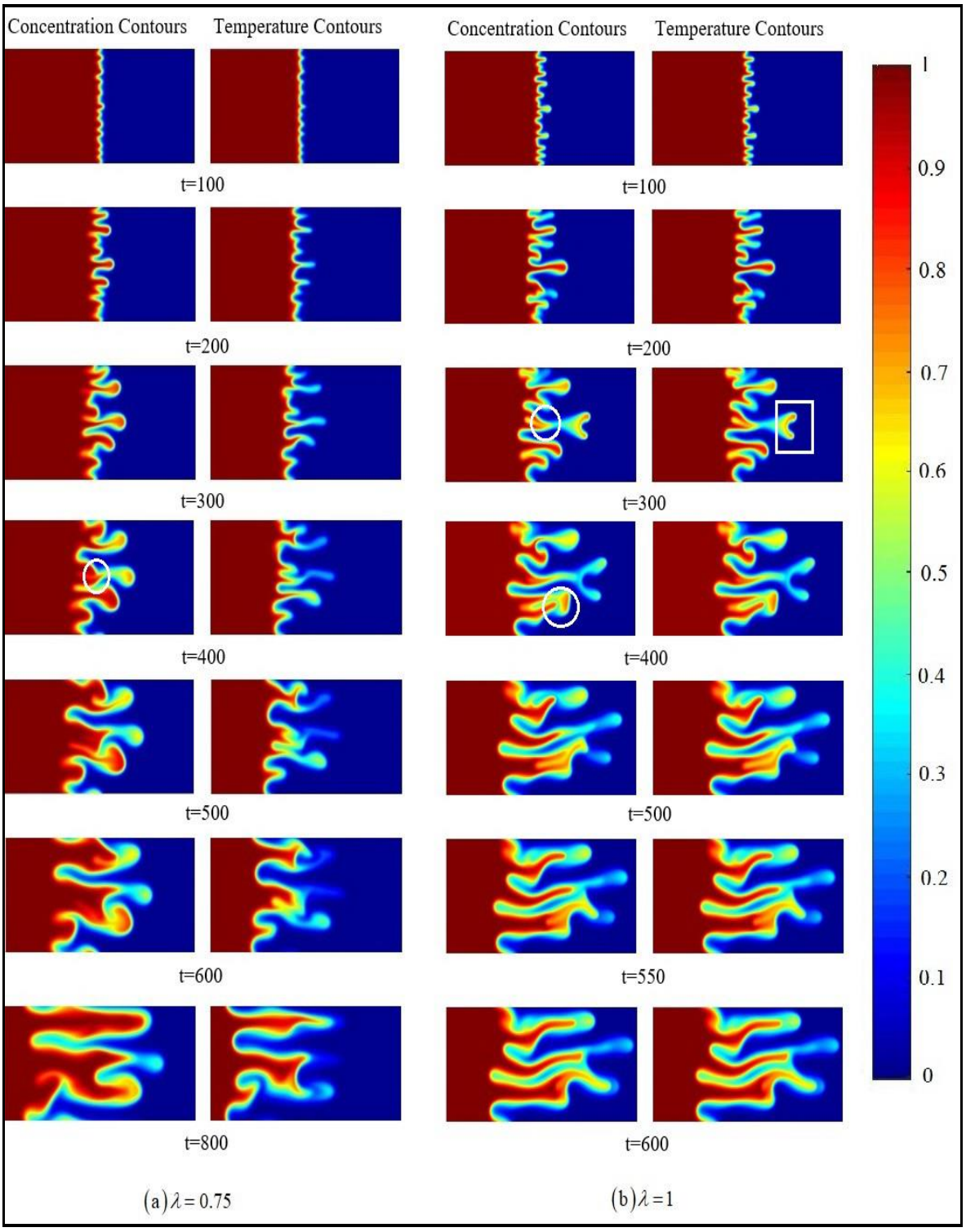

Fig. 7. The effect of the thermal-lag coefficient (λ) on the concentration and temperature contours ($\beta_C = \beta_T = 1.5$).

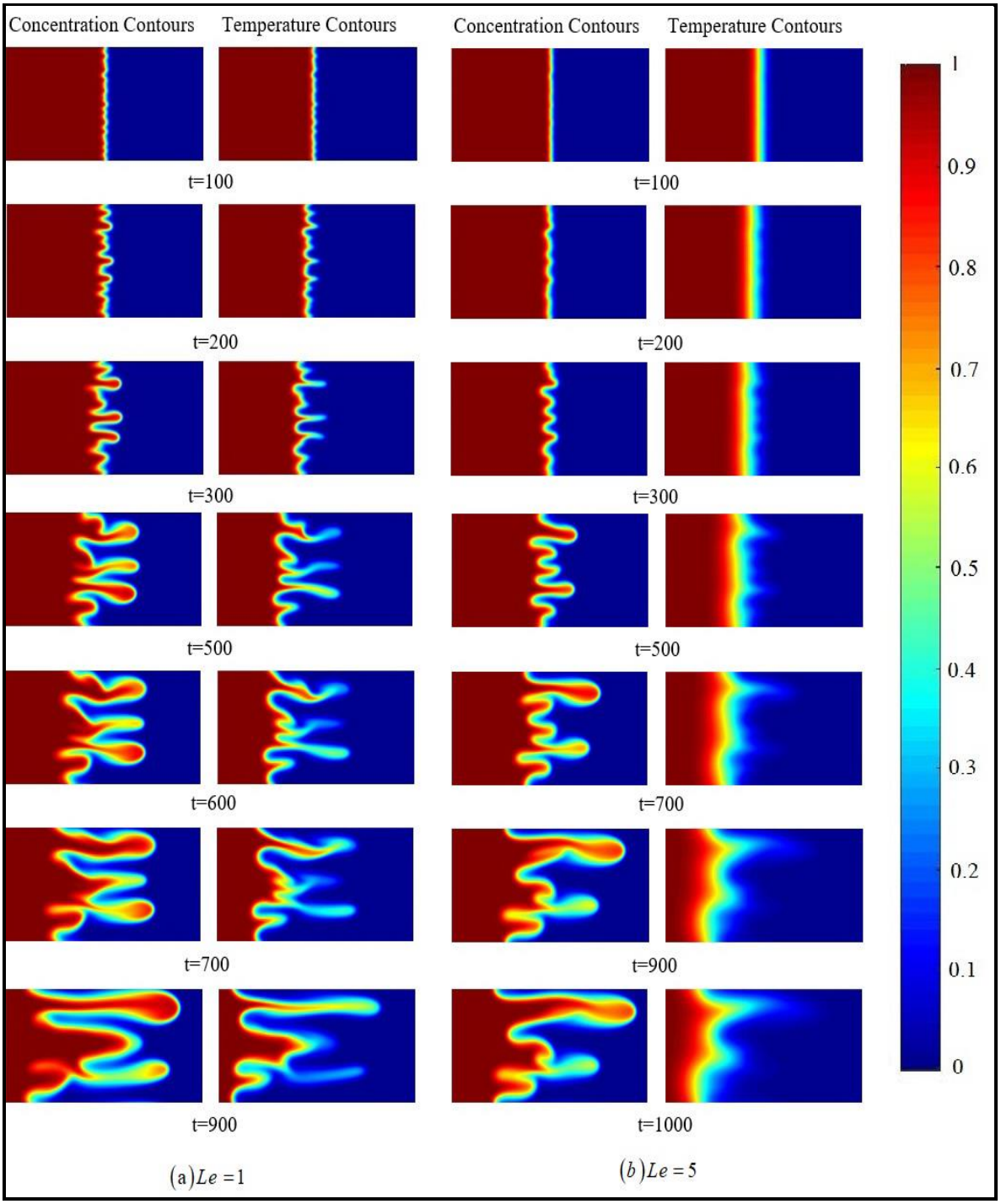

Fig. 8. The effect of the Lewis number (Le) on the concentration and temperature contours ($\beta_C = \beta_T = 1.5$).

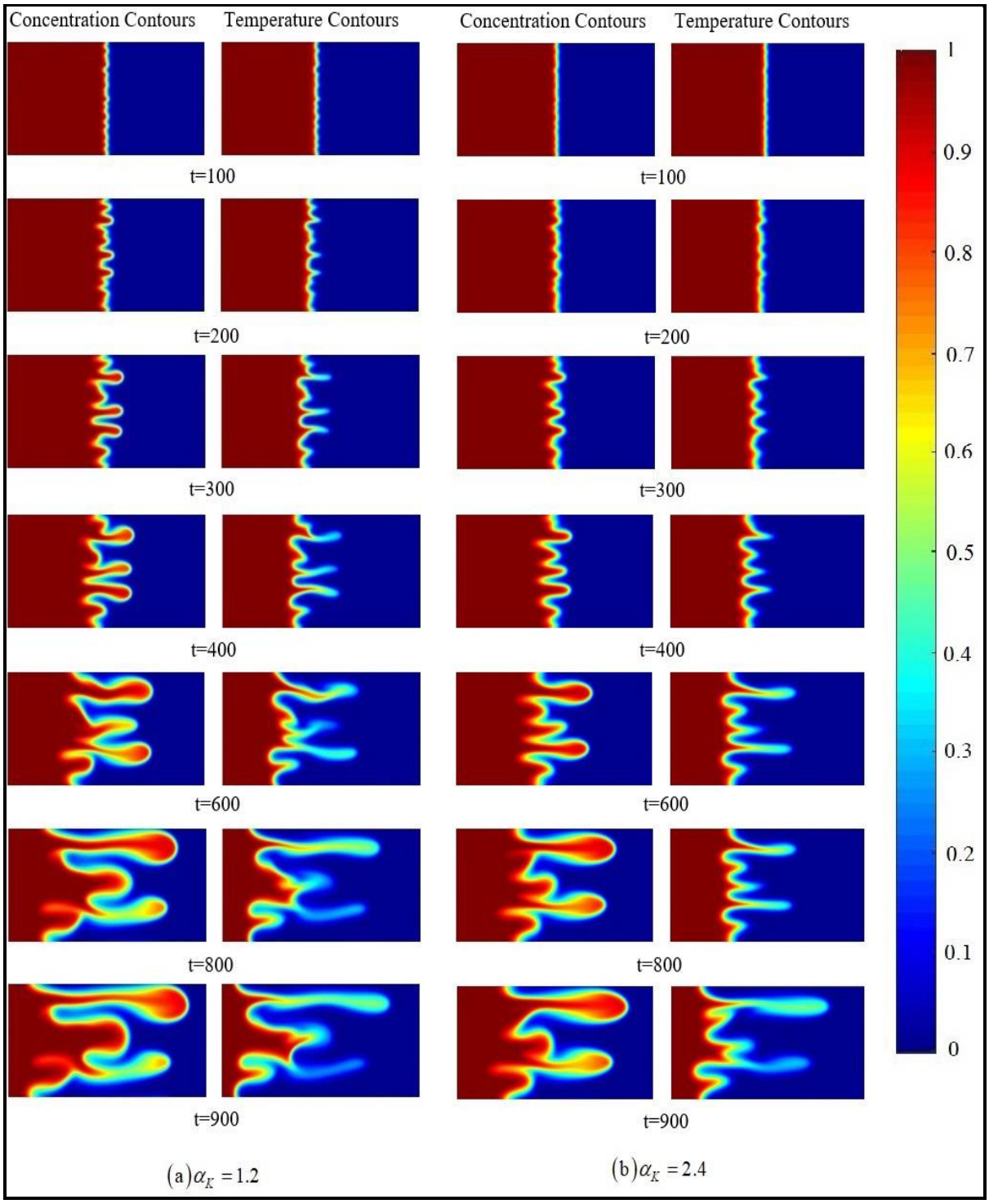

Fig. 9. The effect of the permeability ratio (α_K) on the concentration and temperature contours ($\beta_C = \beta_T = 1.5$).

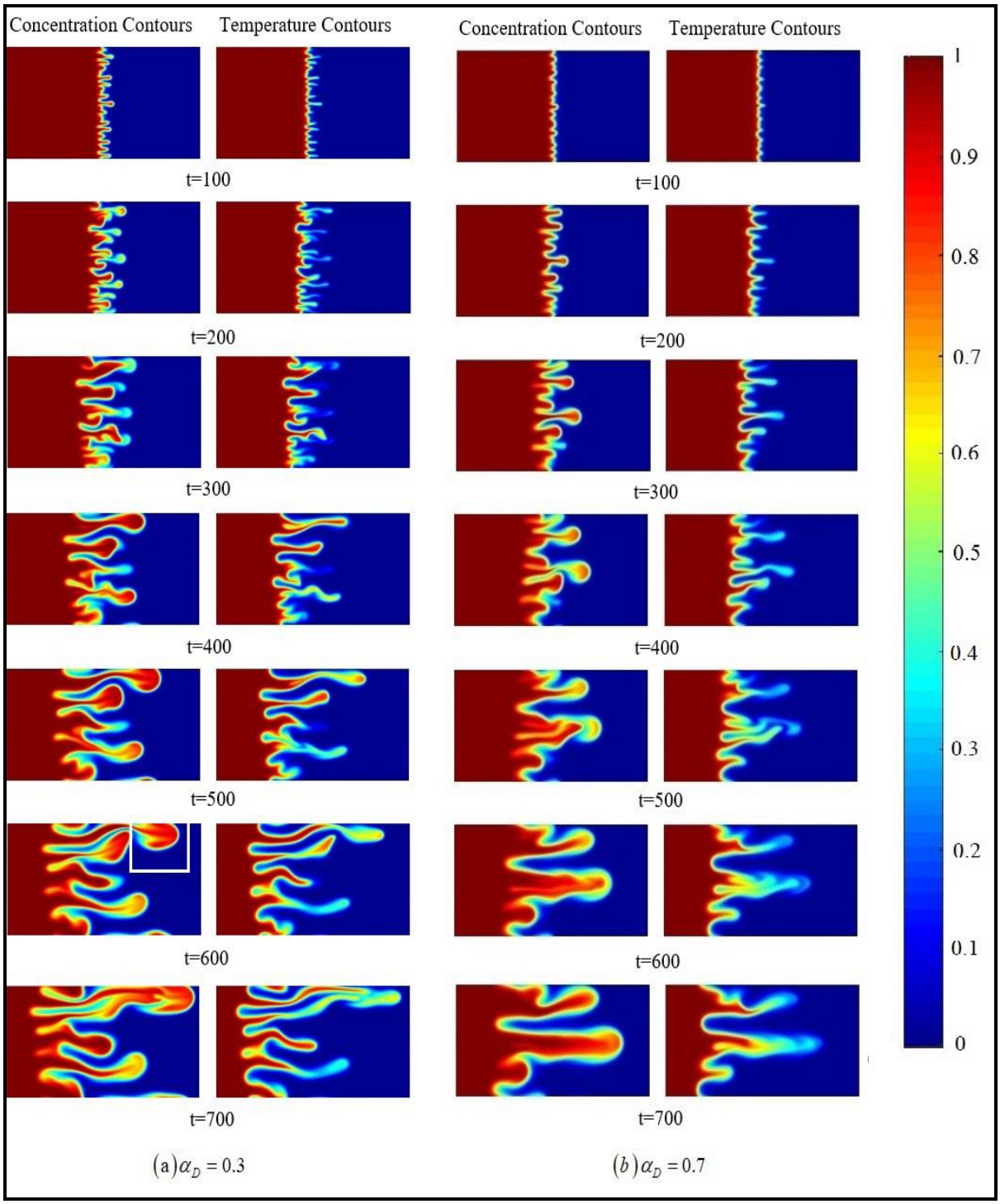

Fig. 10. The effect of the dispersion ratio (α_D) on the concentration and temperature contours ($\beta_C = \beta_T = 1.5$).

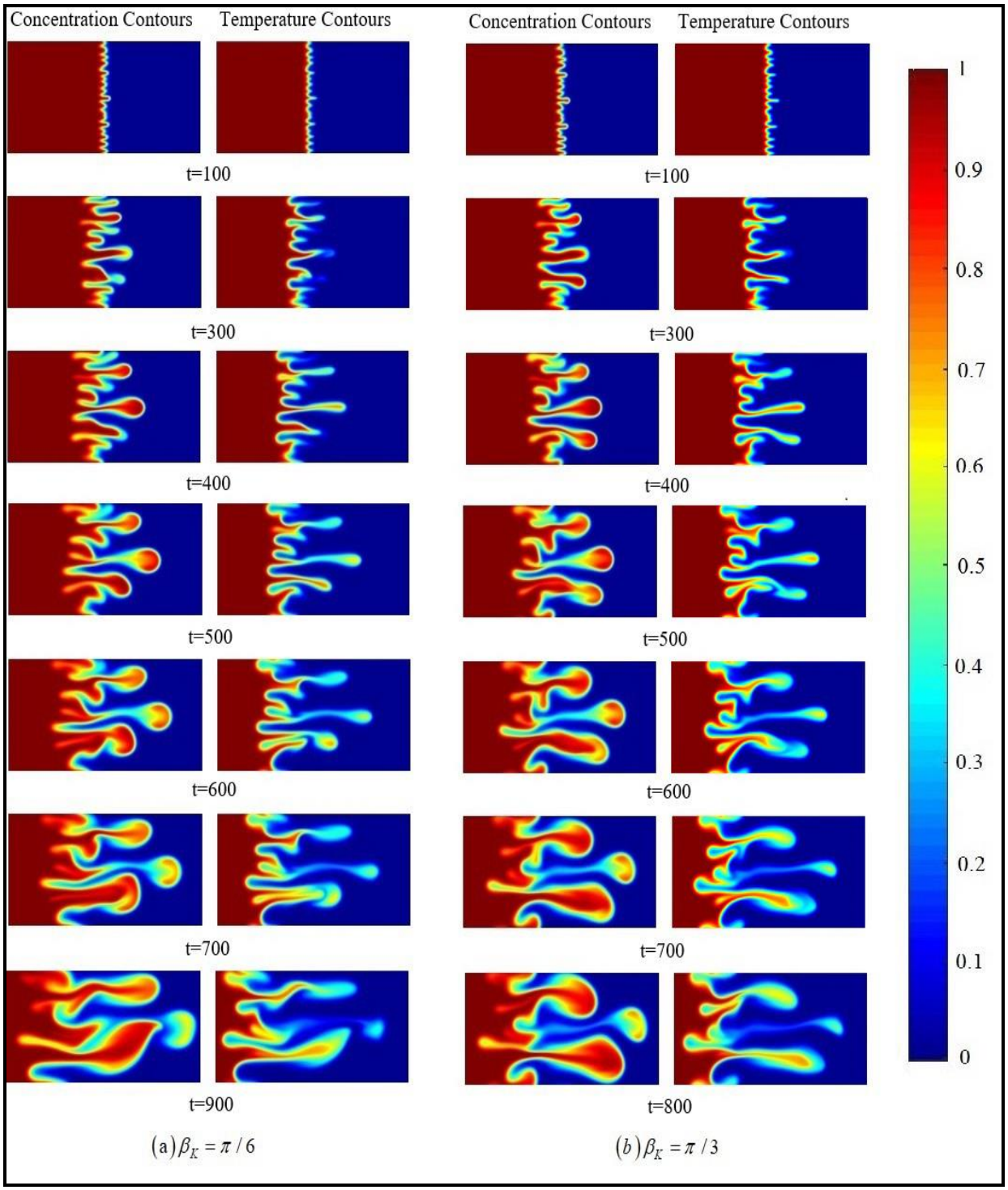

Fig. 11. The effect of permeability angle (β_K) on the concentration and temperature contours ($\beta_C = \beta_T = 1.5$).

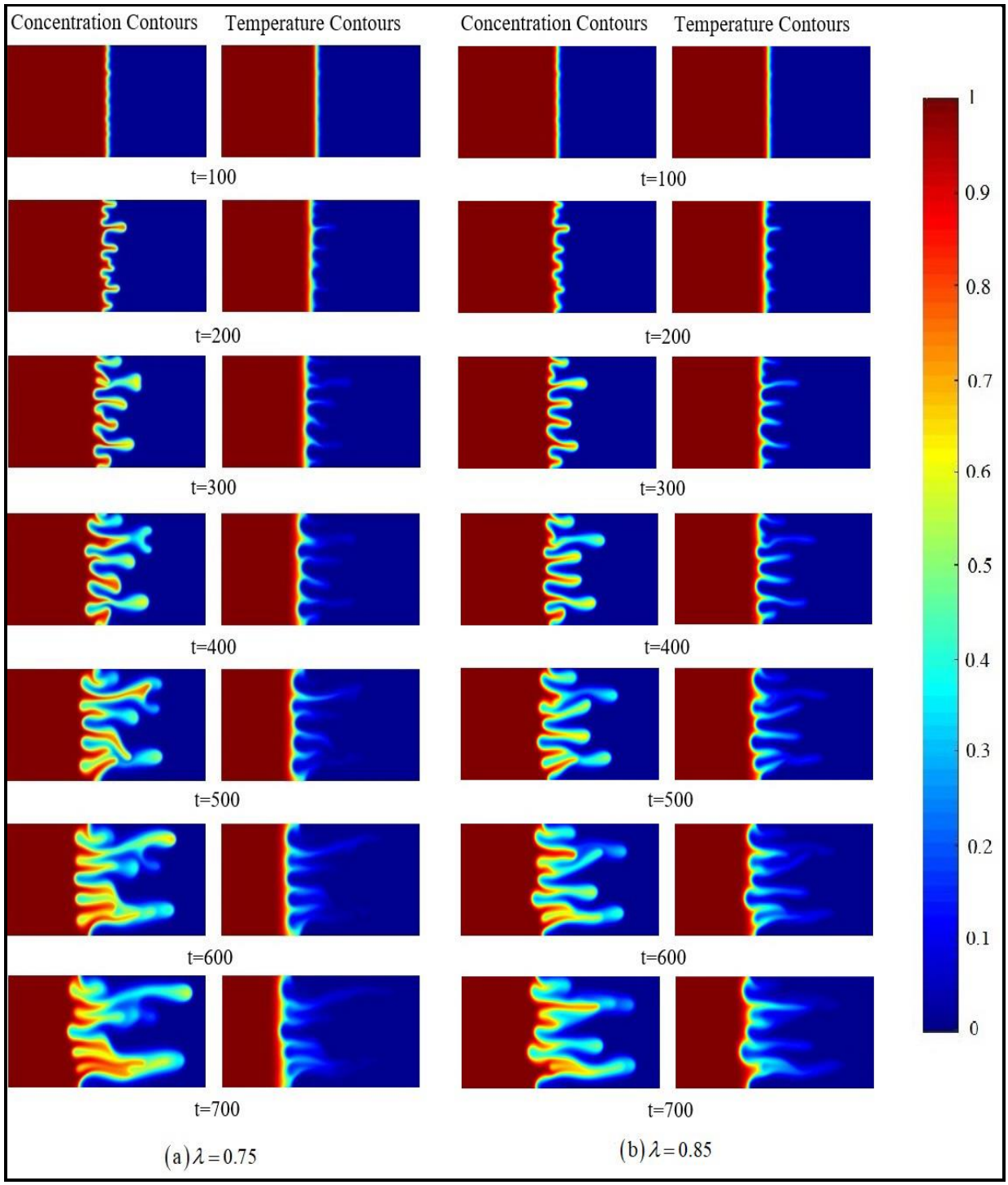

Fig. 12. The effect of the thermal-lag coefficient (λ) on the concentration and temperature contours ($\beta_C = 3$ and $\beta_T = -1.5$).

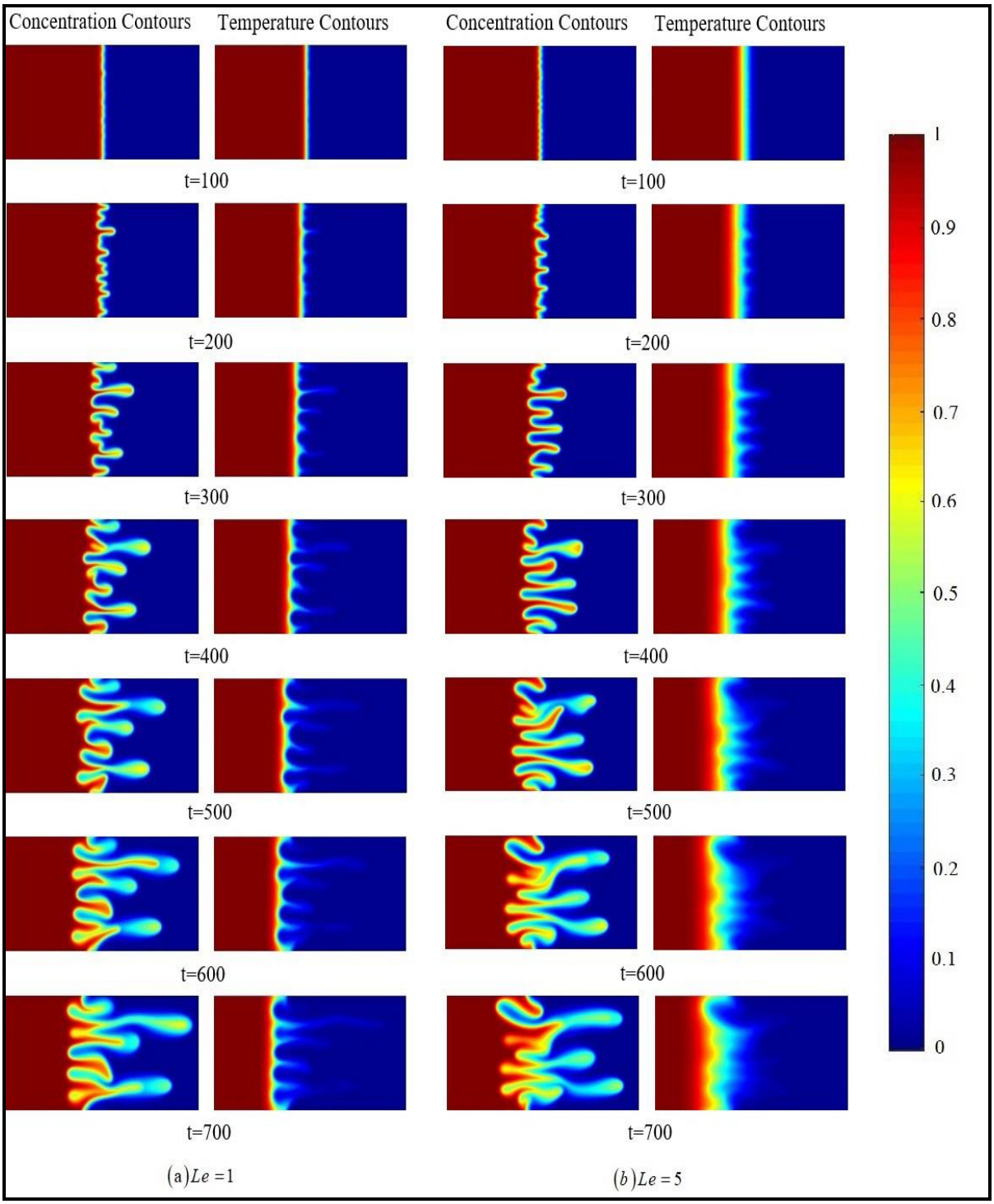

Fig. 13. The effect of the Lewis number (Le) on the concentration and temperature contours ($\beta_C = 3$ and $\beta_T = -1.5$).

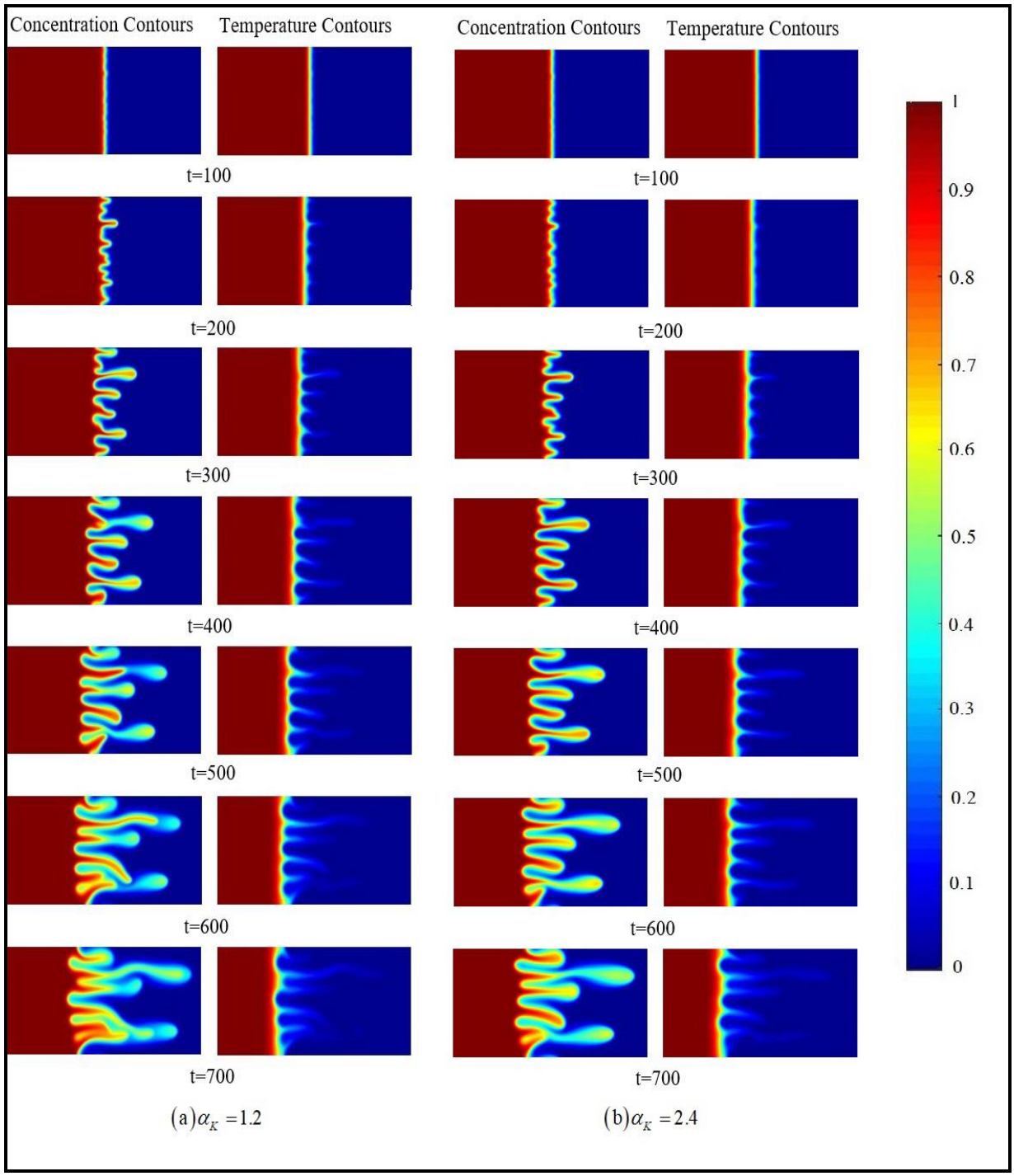

Fig. 14. The effect of the permeability ratio (α_K) on the concentration and temperature contours ($\beta_C = 3$ and $\beta_T = -1.5$).

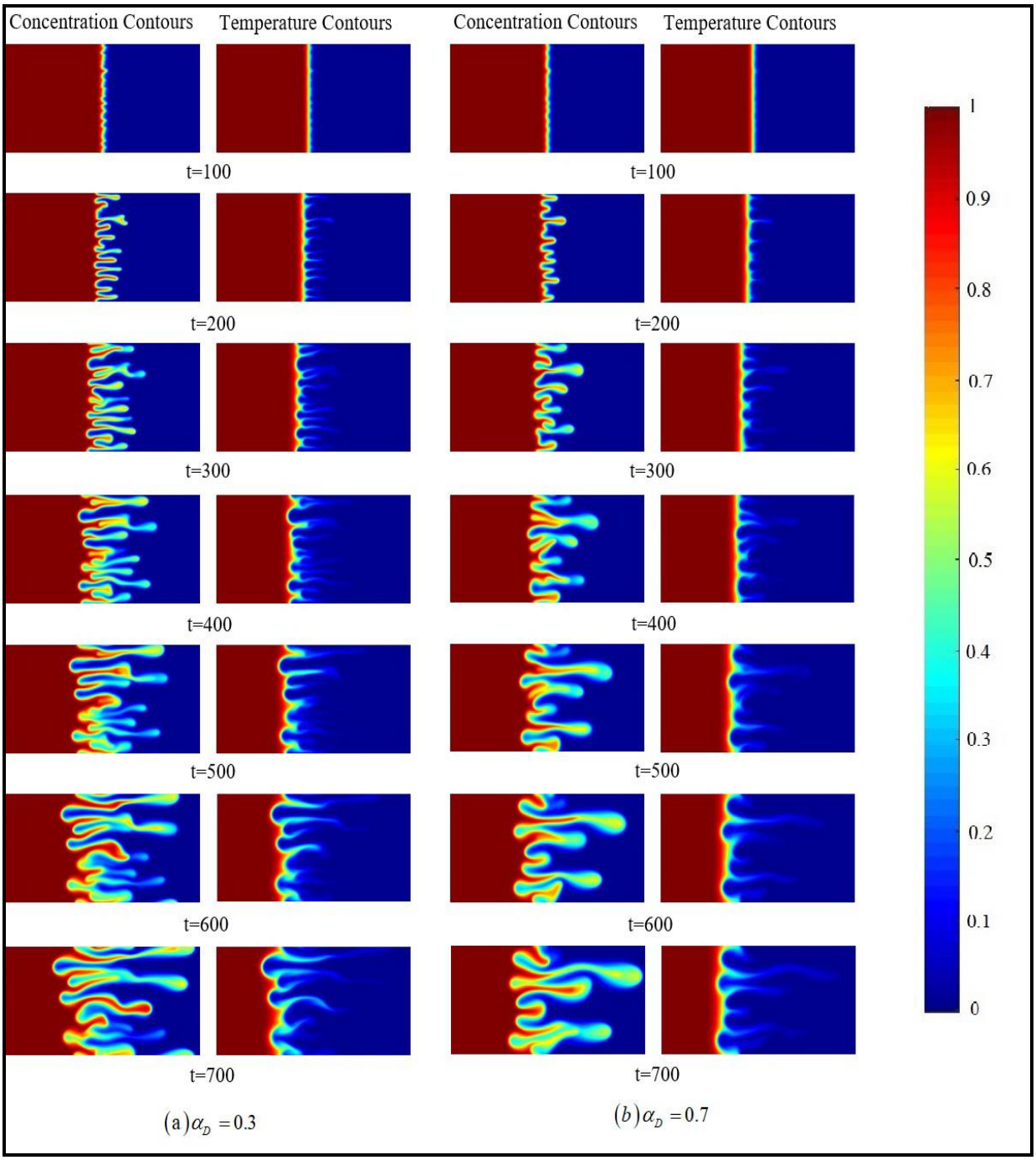

Fig. 15. The effect of the dispersion ratio (α_D) on the concentration and temperature contours ($\beta_C = 3$ and $\beta_T = -1.5$).

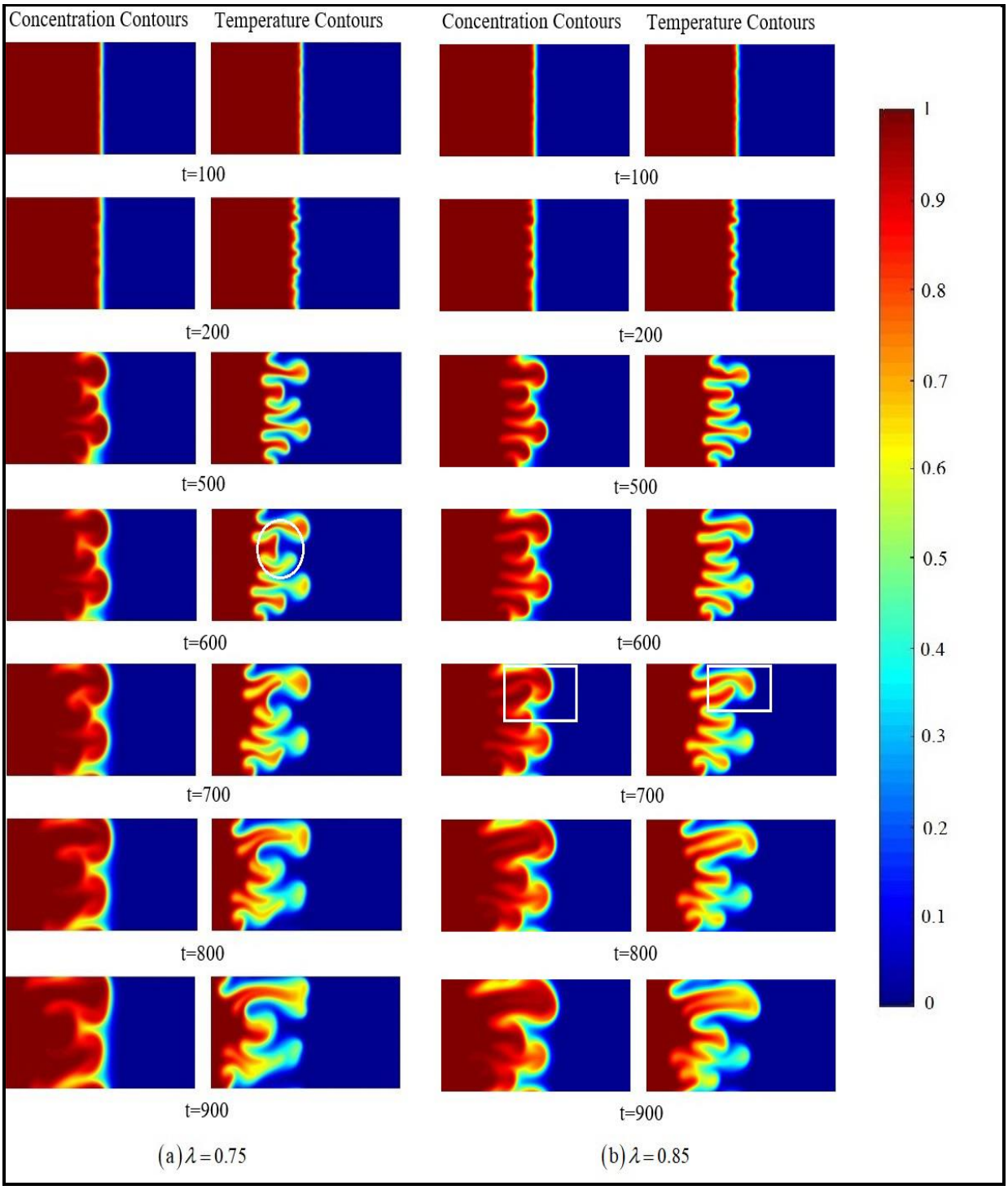

Fig. 16. The effect of the thermal-lag coefficient (λ) on the concentration and temperature contours ($\beta_C = -1.5$ and $\beta_T = 3$).

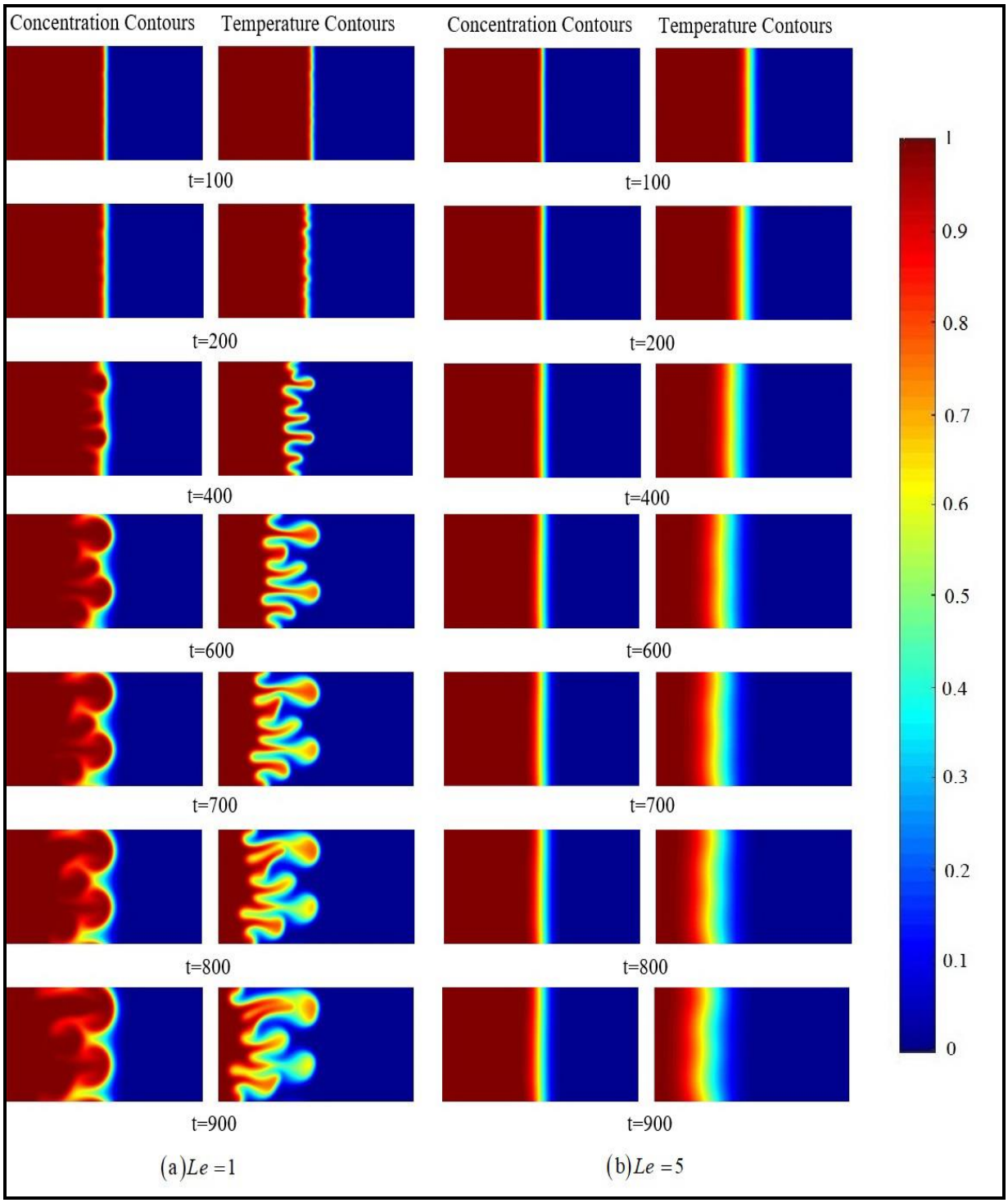

Fig. 17. The effect of the Lewis number (Le) on the concentration and temperature contours ($\beta_C = -1.5$ and $\beta_T = 3$).

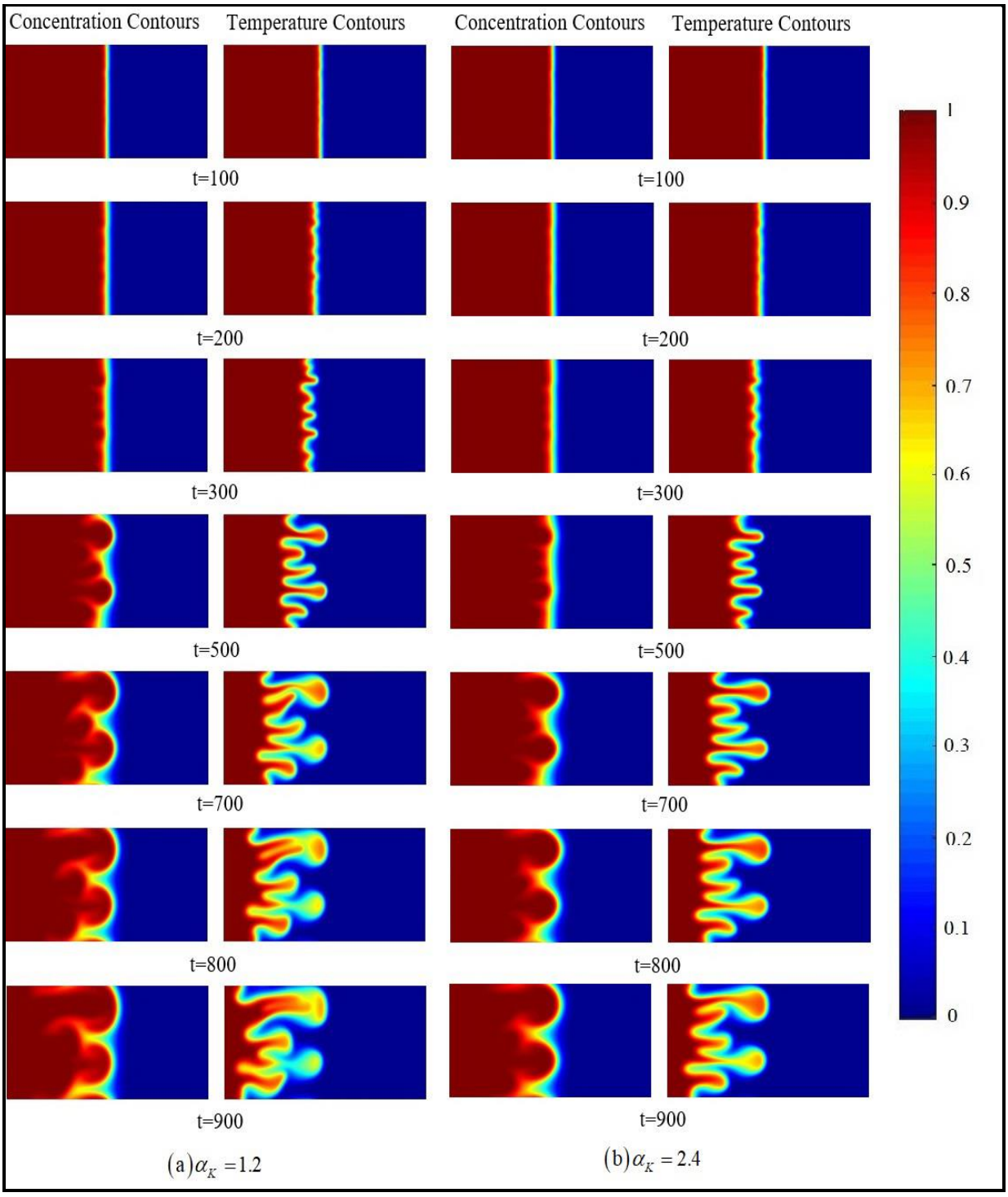

Fig. 18. The effect of the permeability ratio (α_K) on the concentration and temperature contours ($\beta_C = -1.5$ and $\beta_T = 3$).

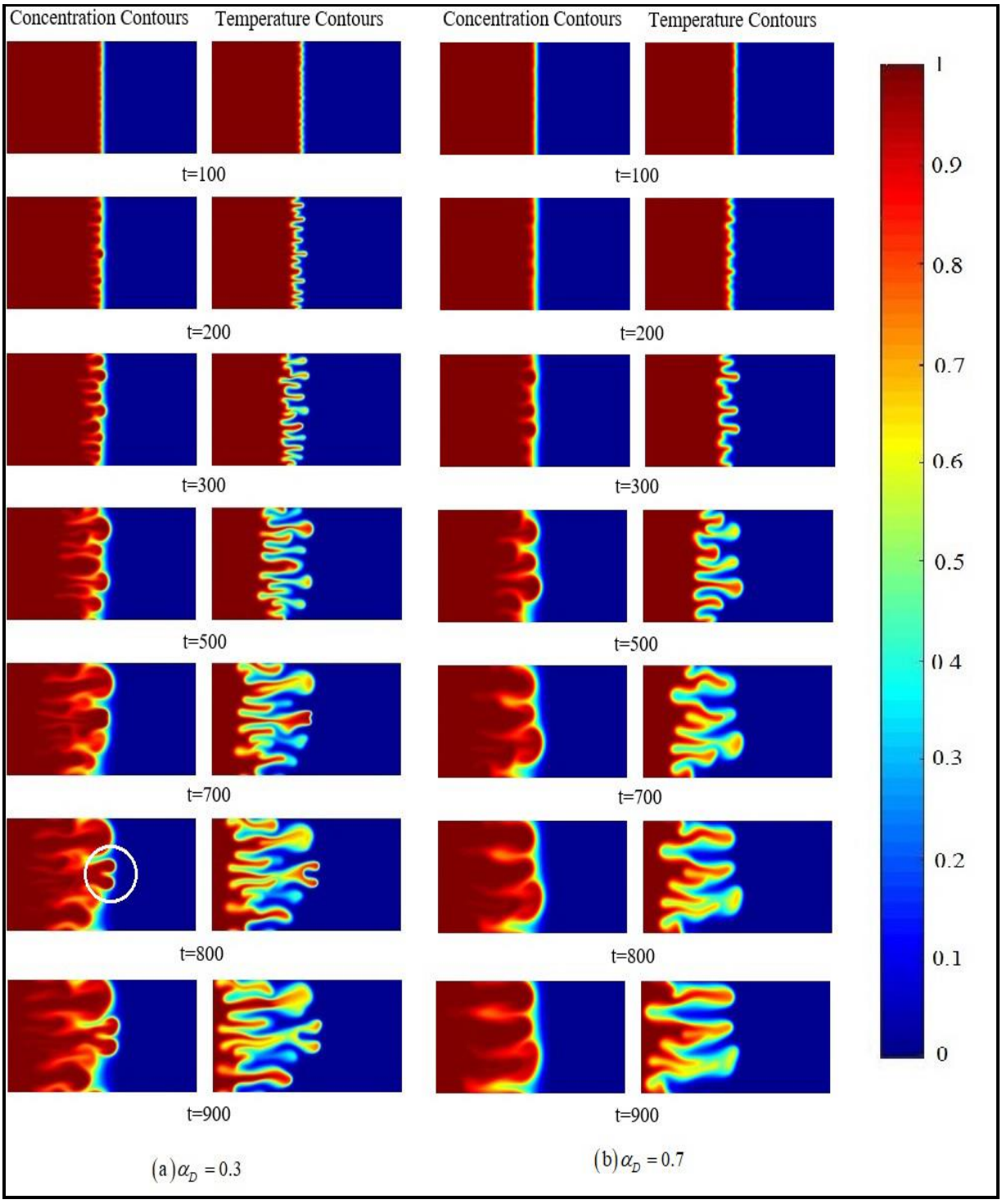

Fig. 19. The effect of the dispersion ratio (α_D) one the concentration and temperature contours ($\beta_C = -1.5$ and $\beta_T = 3$).

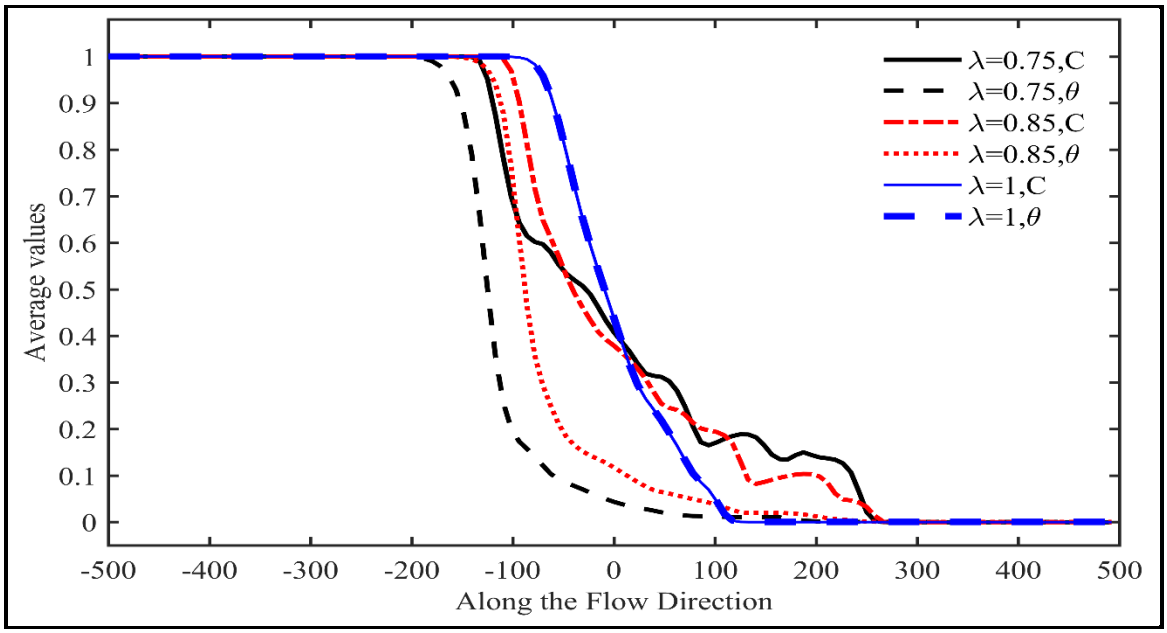

Fig. 20. a. The effect of the thermal-lag coefficient (λ) on the concentration and temperature averaged profiles $\beta_C = 3$ and $\beta_T = -1.5$

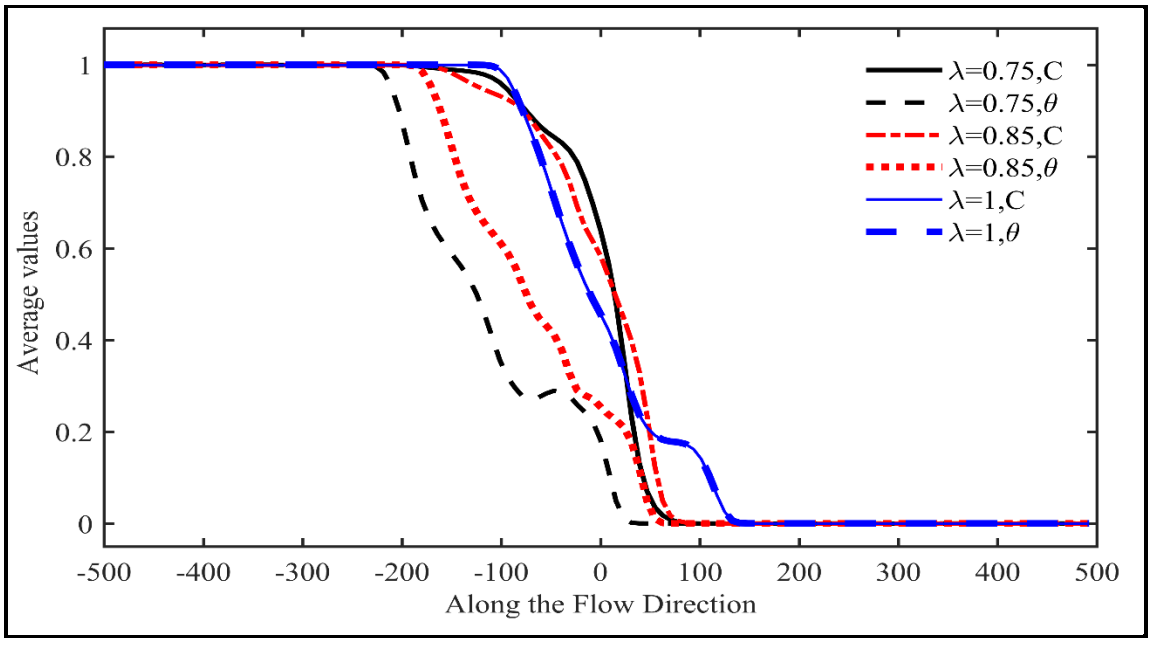

Fig. 20. b. The effect of the thermal-lag coefficient (λ) on the concentration and temperature averaged profiles $\beta_C = -1.5$ and $\beta_T = 3$

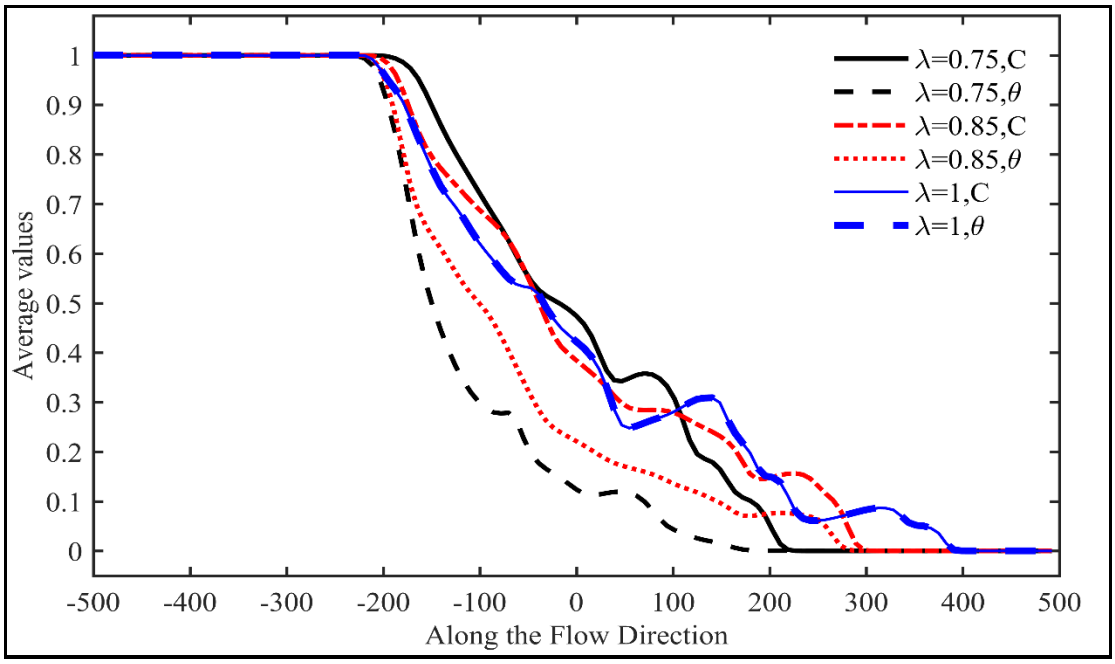

Fig. 20. c The effect of the thermal-lag coefficient (λ) on the concentration and temperature averaged profiles $\beta_C = \beta_T = 1.5$.

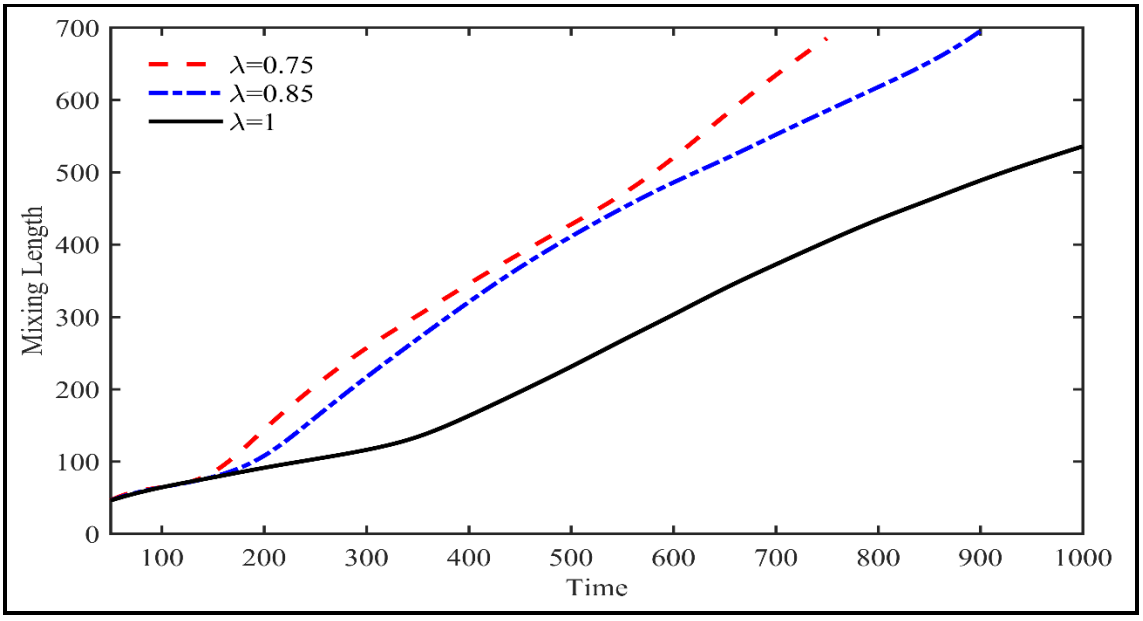

Fig.21. a. The effect of the thermal-lag coefficient (λ) on the mixing length $\beta_C = 3$ and $\beta_T = -1.5$

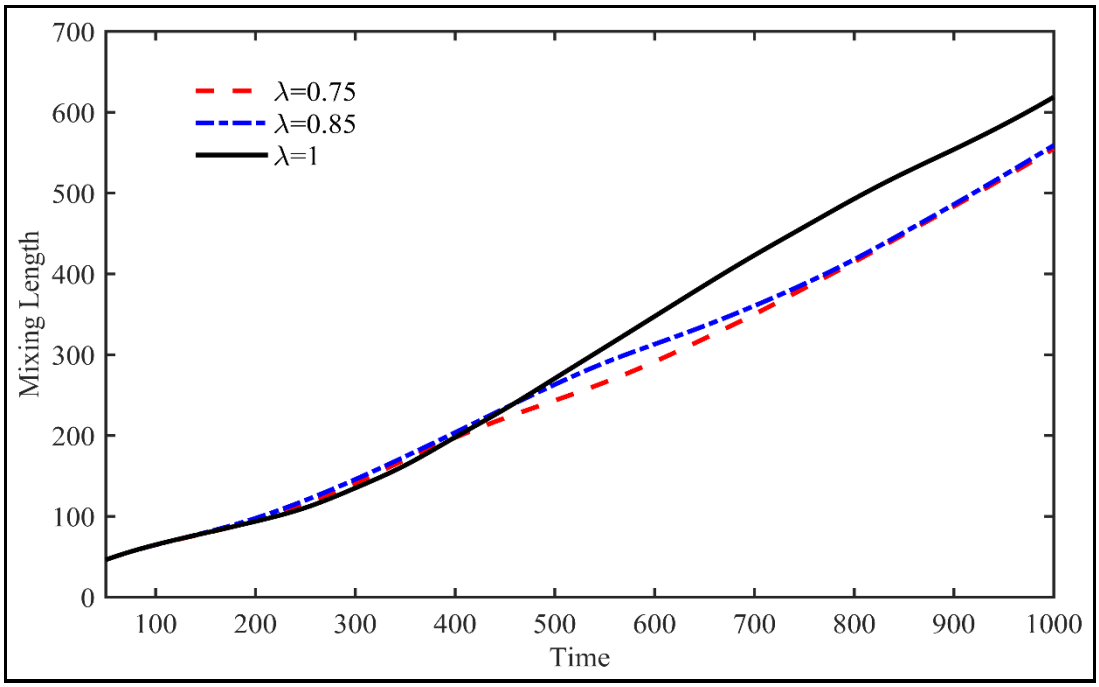

Fig.21. b. The effect of the thermal-lag coefficient (λ) on the mixing length $\beta_C = -1.5$ and $\beta_T = 3$

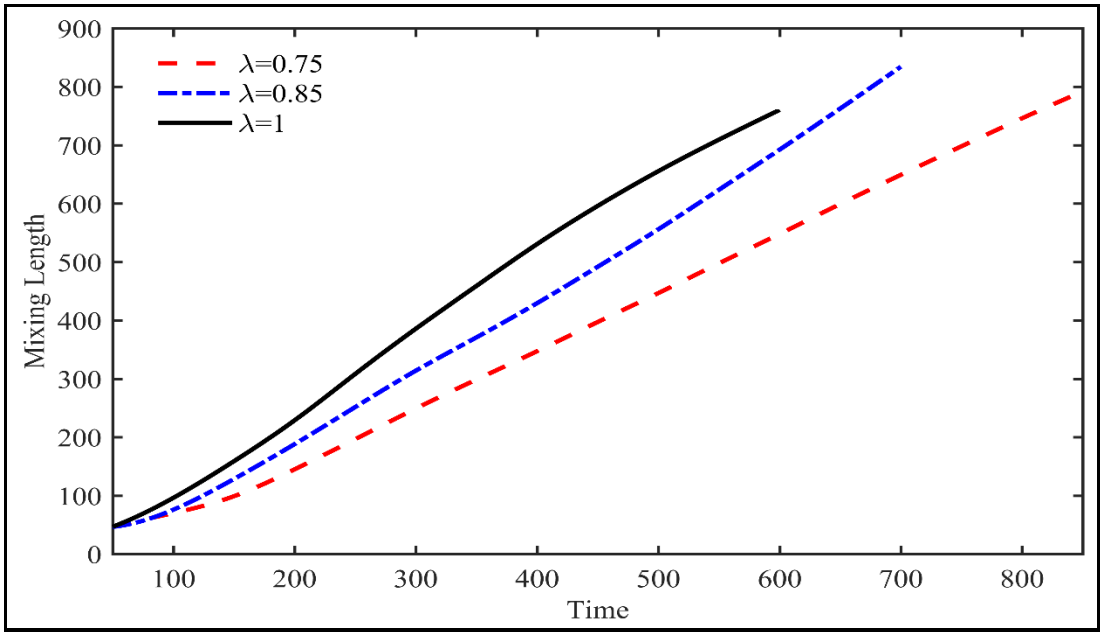

Fig.21. c. The effect of the thermal-lag coefficient (λ) on the mixing length $\beta_C = \beta_T = 1.5$.

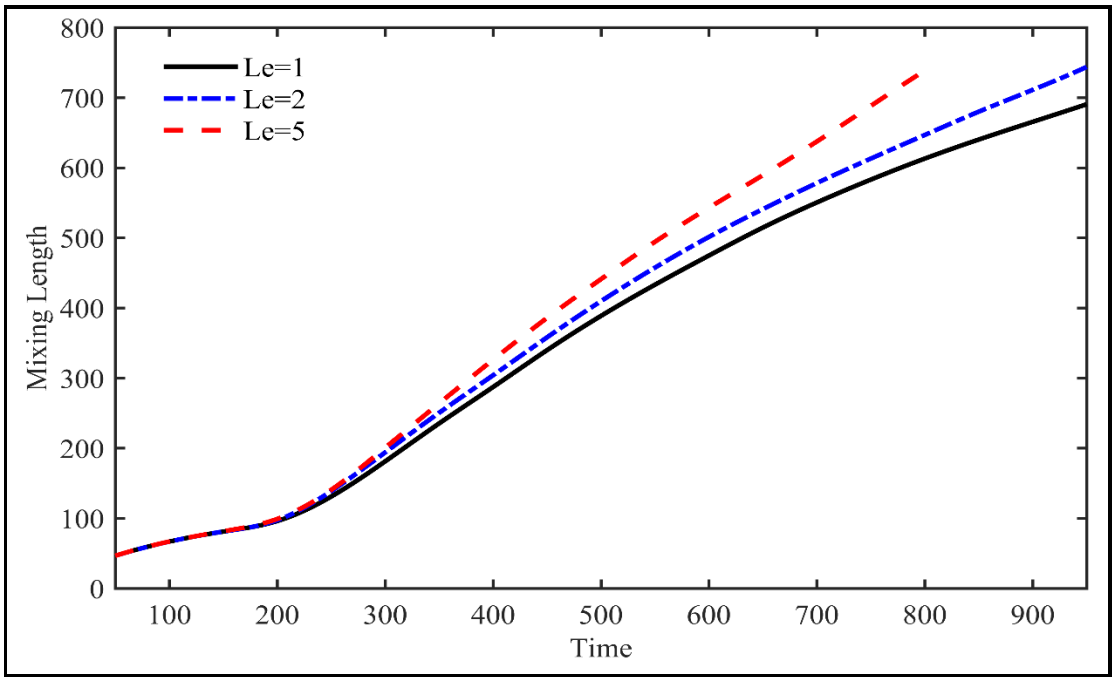

Fig. 22. a. The effect of the Lewis number (Le) on the mixing length $\beta_C = 3$ and $\beta_T = -1.5$

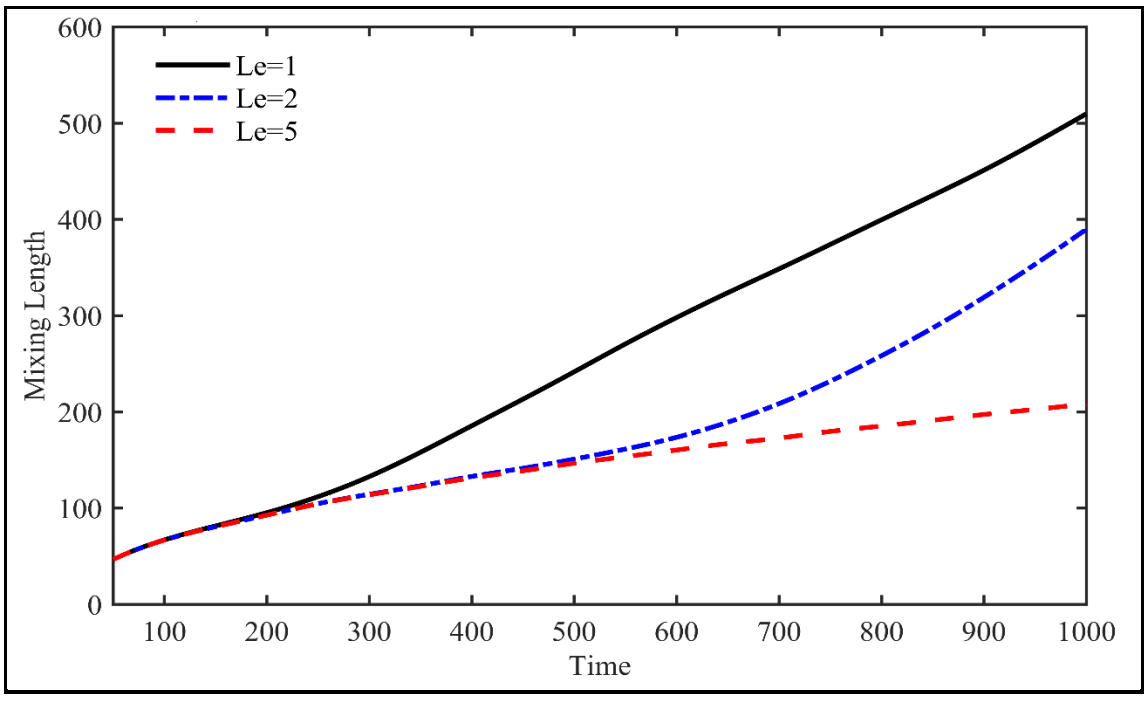

Fig. 22.b. The effect of the Lewis number (Le) on the mixing length $\beta_C = -1.5$ and $\beta_T = 3$,

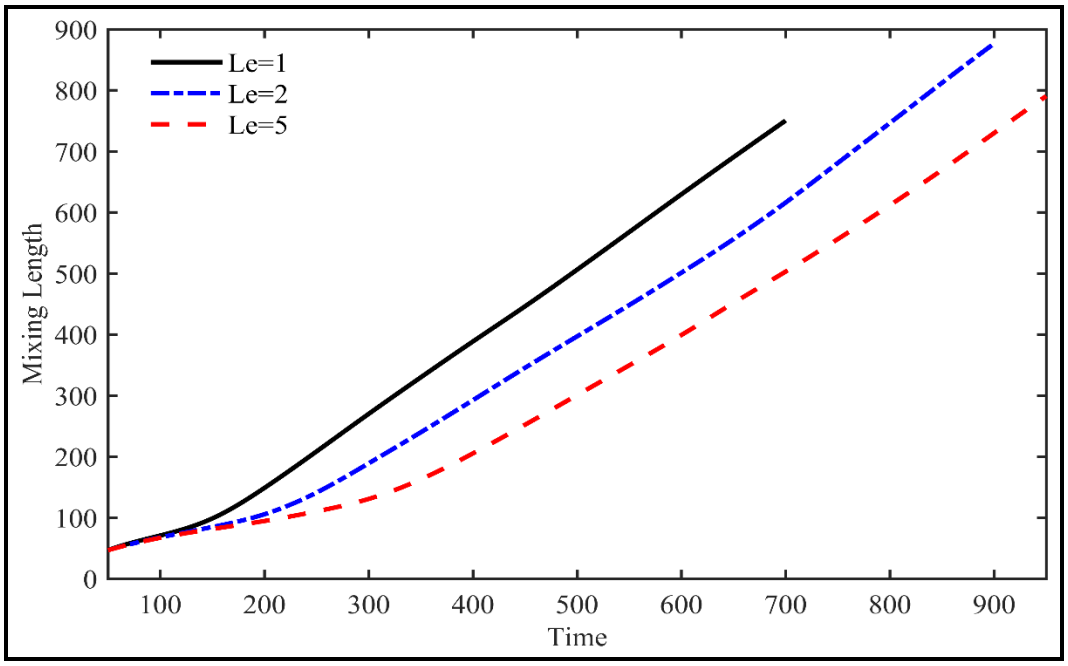

Fig. 22.c. The effect of the Lewis number (Le) on the mixing length $\beta_C = \beta_T = 1.5$.

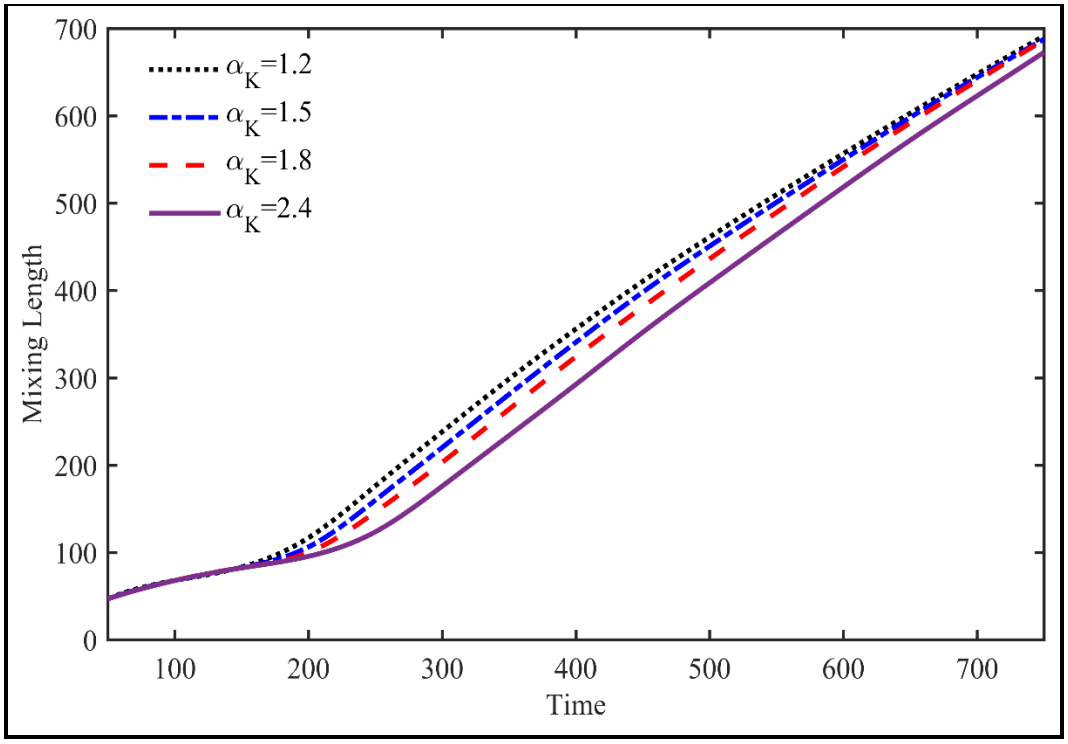

Fig. 23. a. The effect of the permeability ratio (α_K) on the mixing length $\beta_C = 3$ and $\beta_T = -1.5$

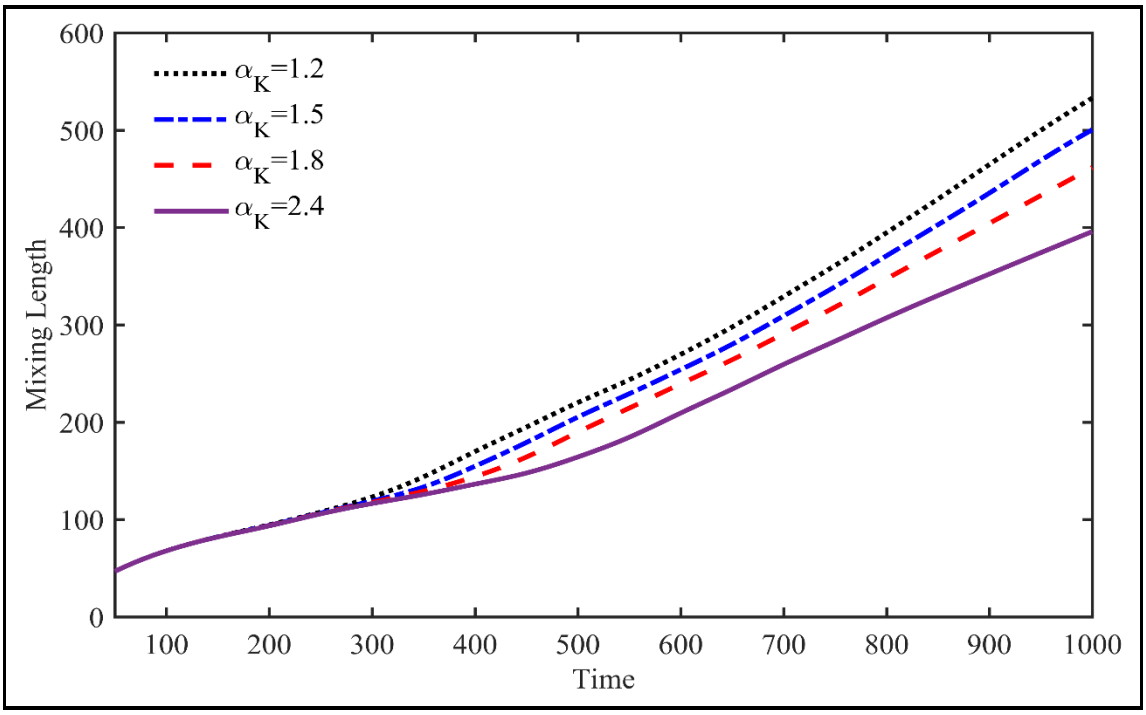

Fig. 23.b. The effect of the permeability ratio (α_K) on the mixing length $\beta_C = -1.5$ and $\beta_T = 3$.

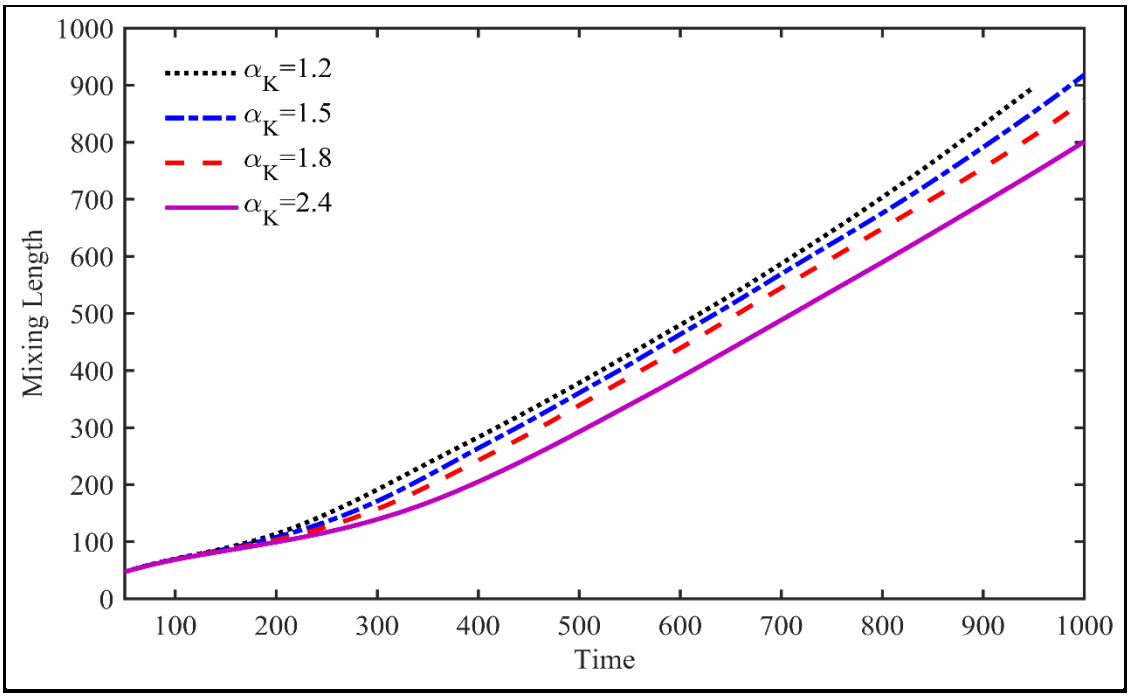

Fig. 23.c. The effect of the permeability ratio (α_K) on the mixing length $\beta_C = \beta_T = 1.5$.

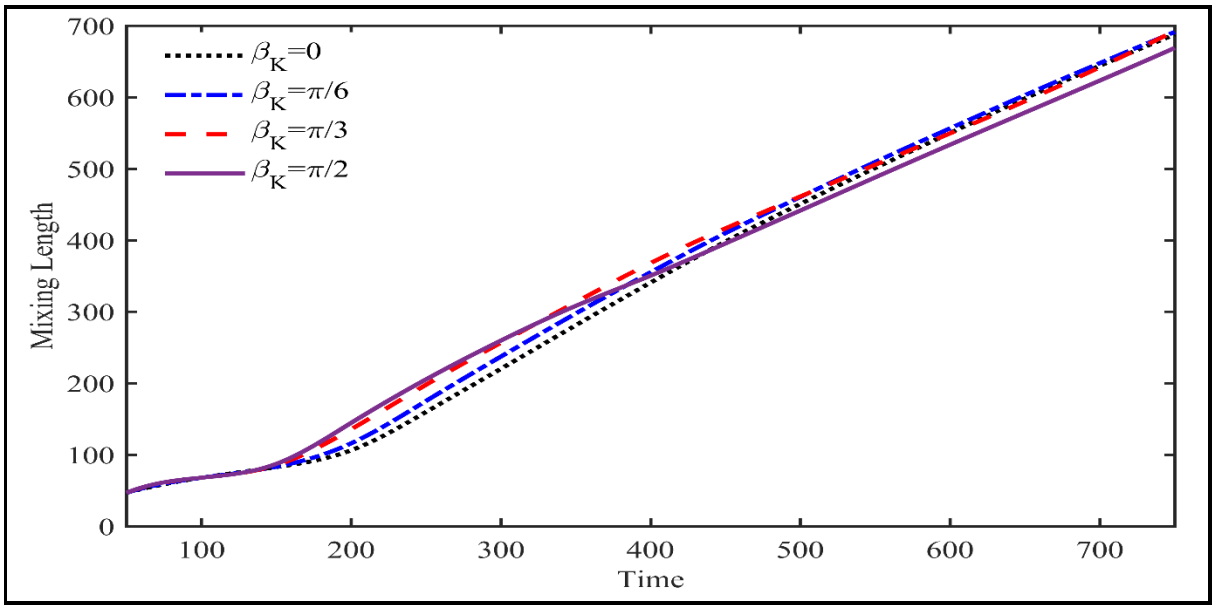

Fig. 24.a. The effect of the permeability angle (β_K) on the mixing length $\beta_C = 3$ and $\beta_T = -1.5$

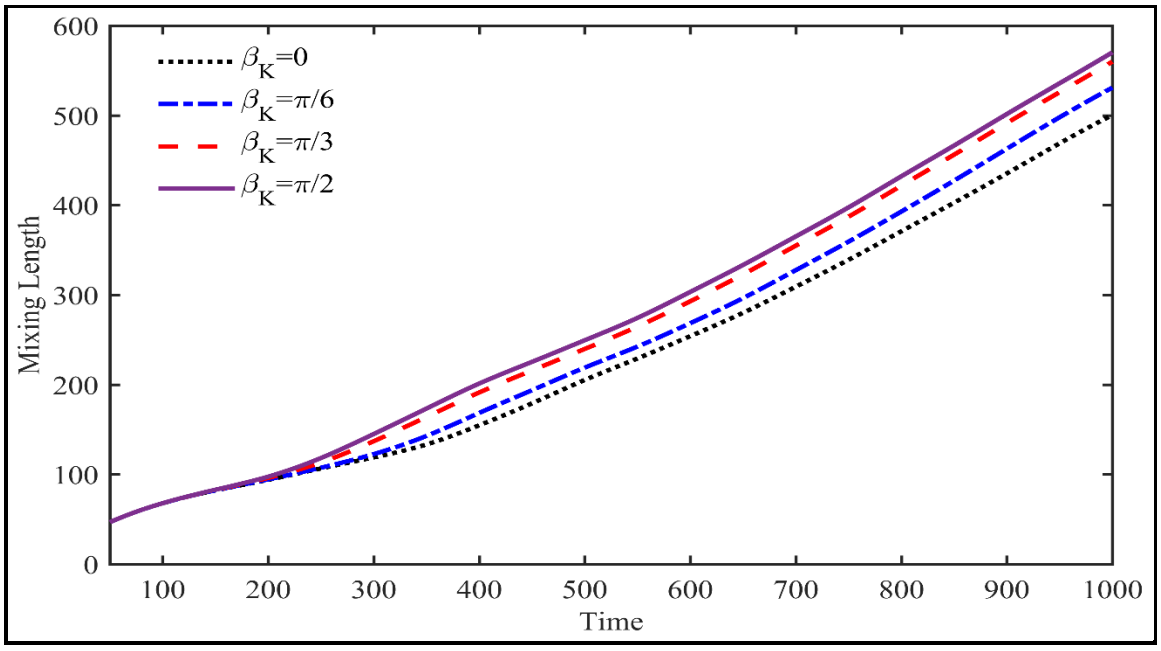

Fig. 24.b. The effect of the permeability angle (β_K) on the mixing length $\beta_C = -1.5$ and $\beta_T = 3$

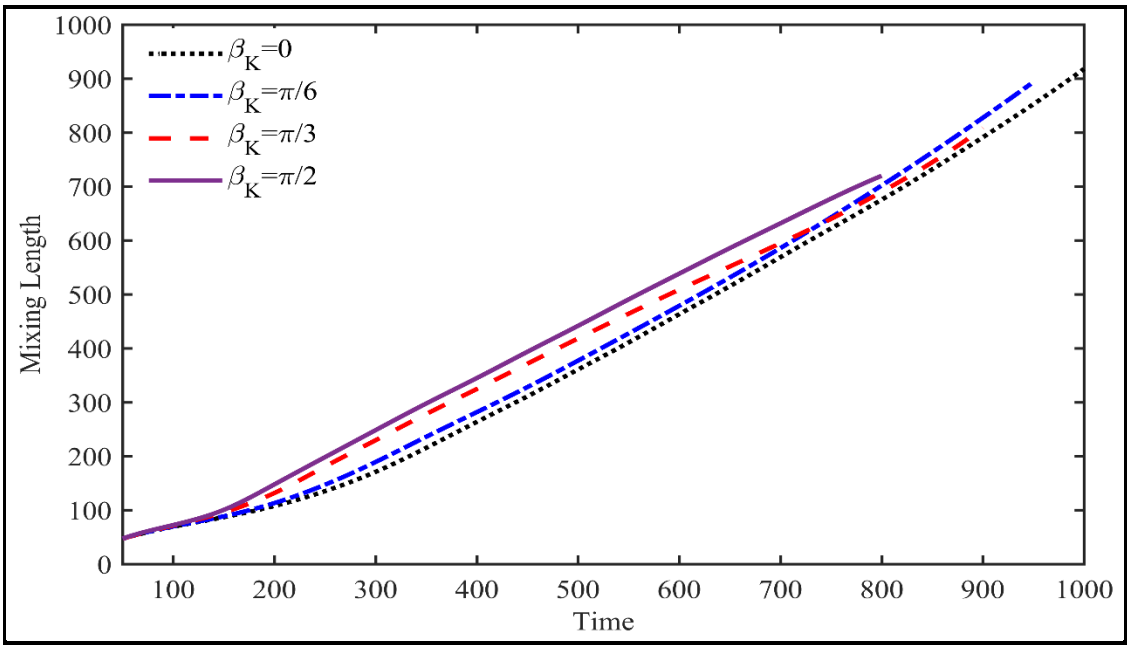

Fig. 24.c. The effect of the permeability angle (β_K) on the mixing length $\beta_C = \beta_T = 1.5$.

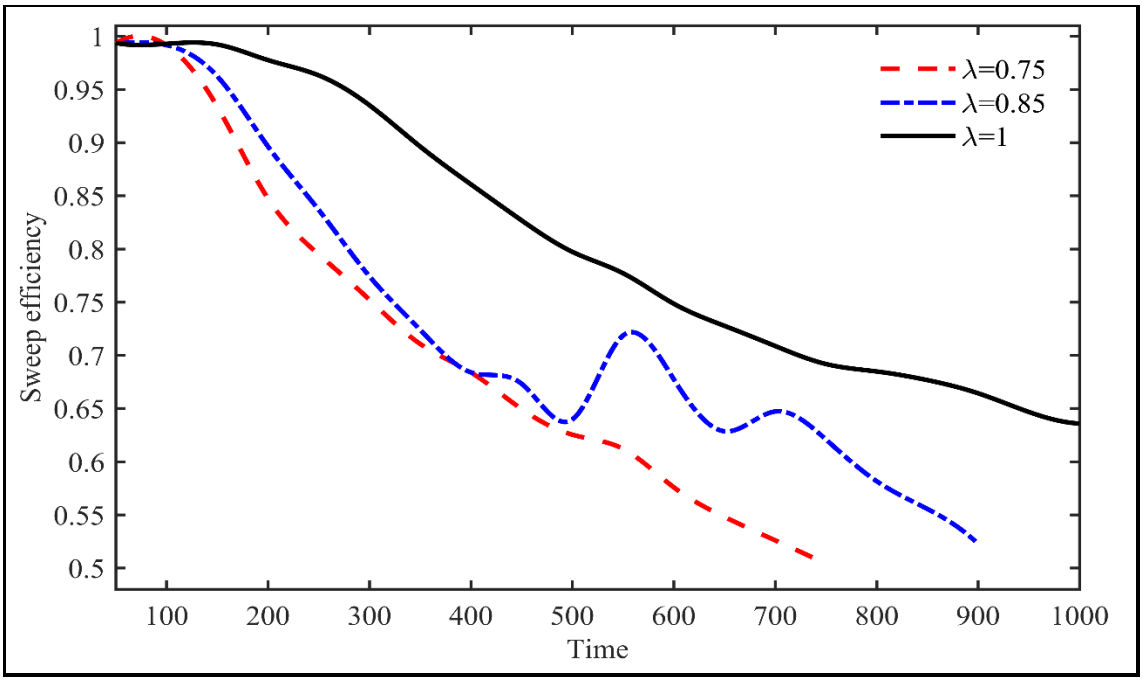

Fig. 25.a. The effect of the thermal-lag coefficient (λ) on the sweep efficiency $\beta_C = 3$ and $\beta_T = -1.5$.

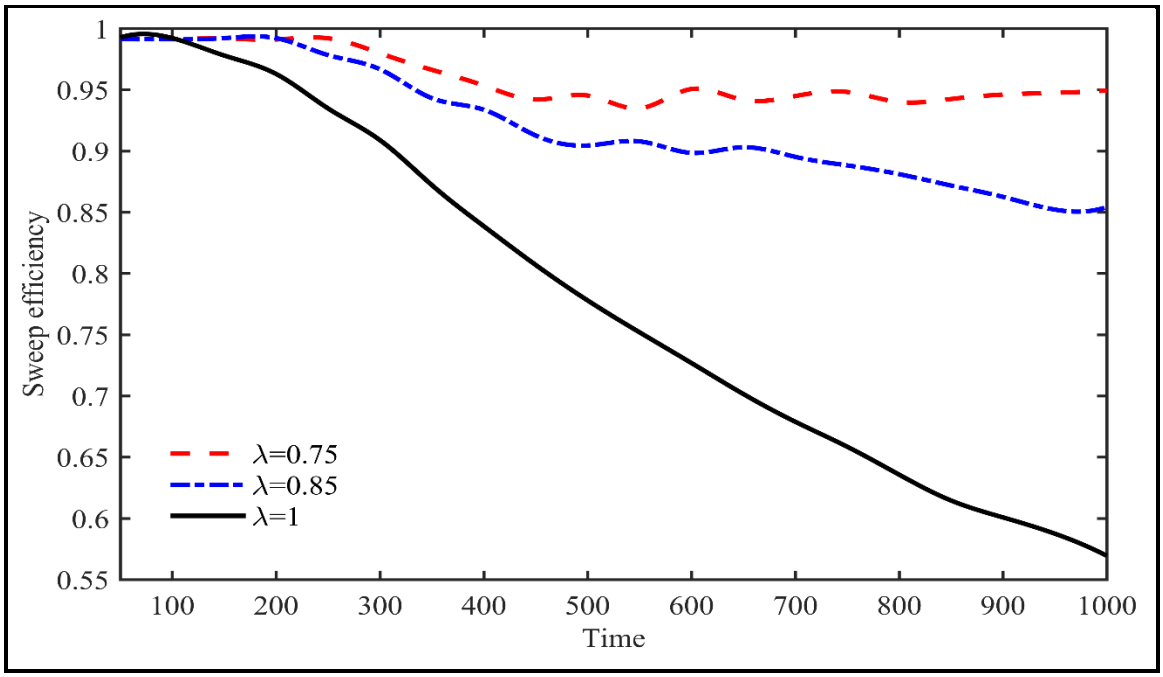

Fig. 25.b. The effect of the thermal-lag coefficient (λ) on the sweep efficiency $\beta_C = -1.5$ and $\beta_T = 3$.

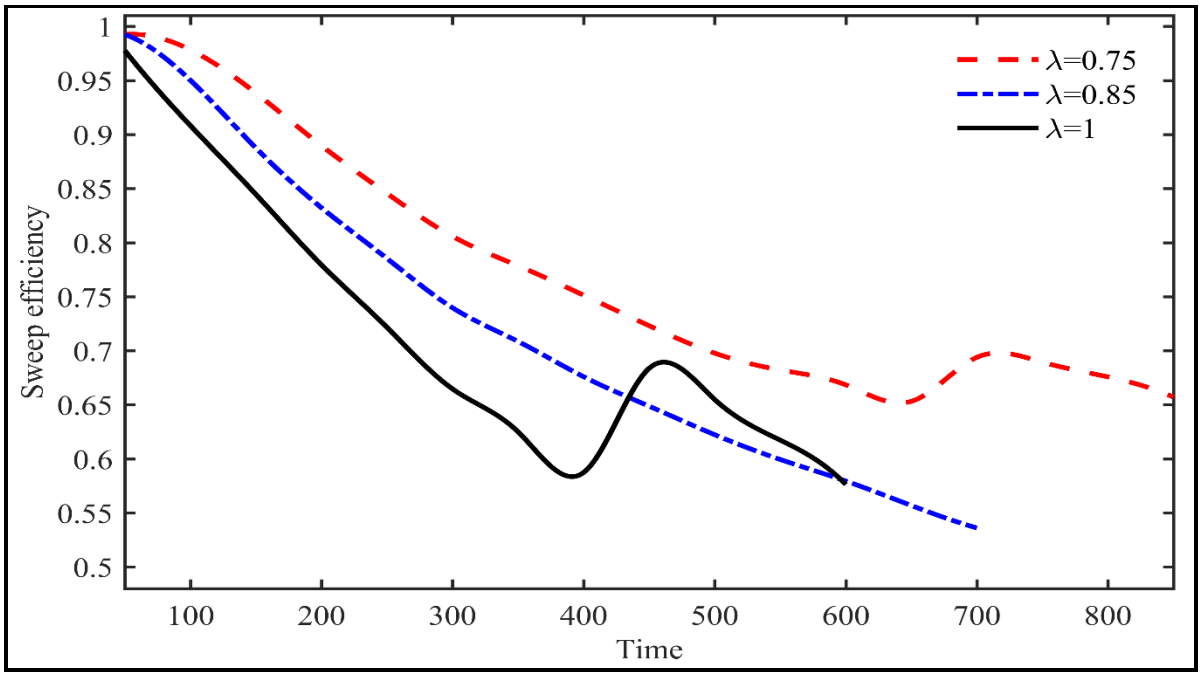

Fig. 25.c. The effect of the thermal-lag coefficient (λ) on the sweep efficiency $\beta_C = \beta_T = 1.5$

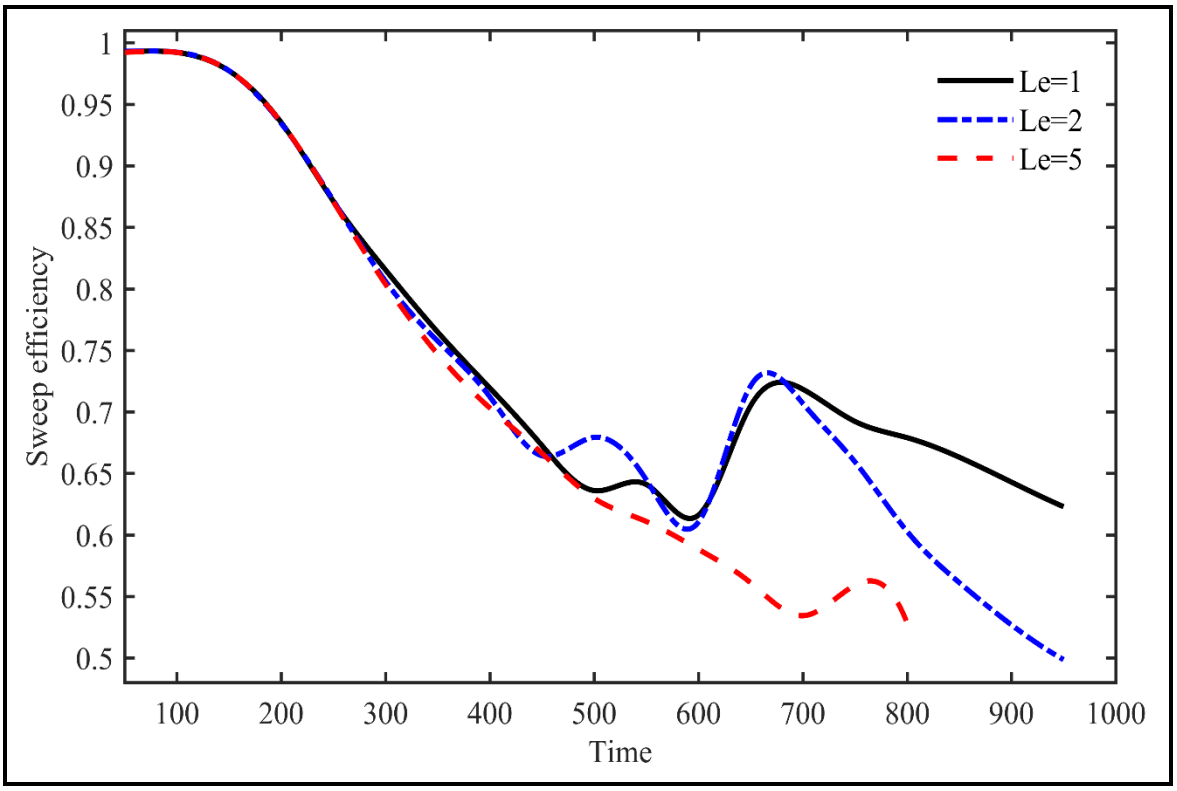

Fig. 26.a. The effect of the Lewis number (Le) on the sweep efficiency $\beta_C = 3$ and $\beta_T = -1.5$.

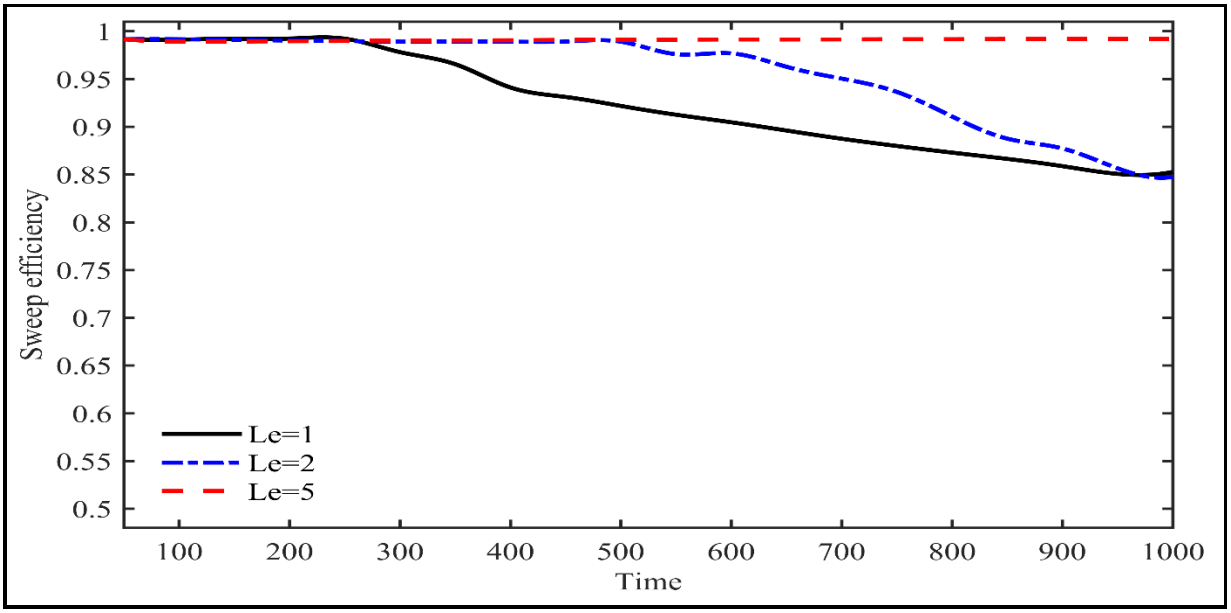

Fig. 26.b. The effect of the Lewis number (Le) on the sweep efficiency $\beta_C = -1.5$ and $\beta_T = 3$.

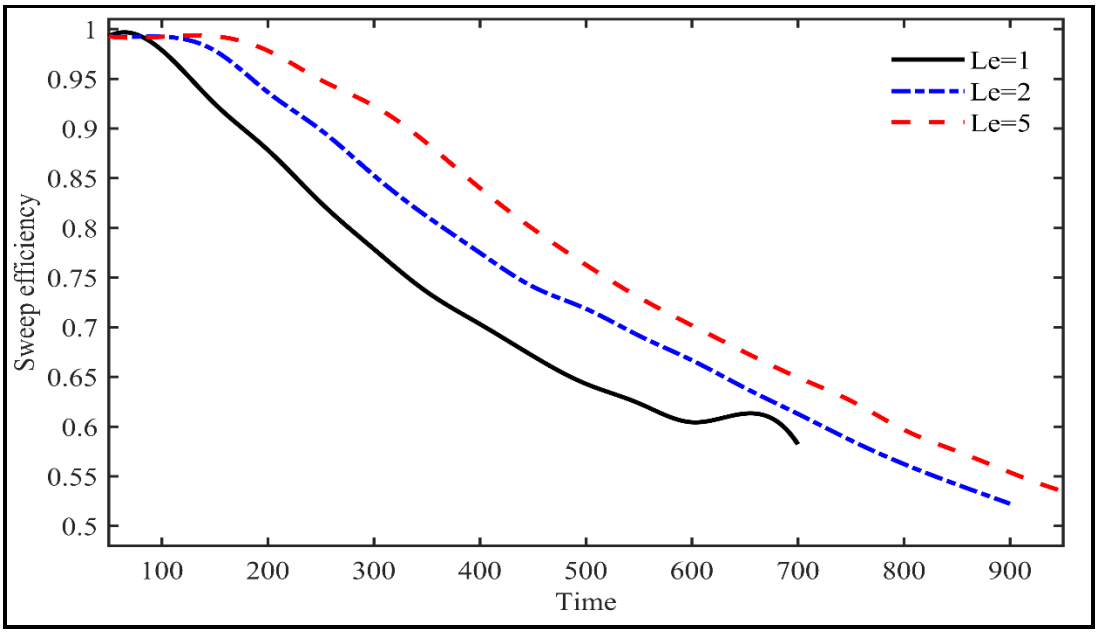

Fig. 26.c. The effect of the Lewis number (Le) on the sweep efficiency $\beta_C = \beta_T = 1.5$.

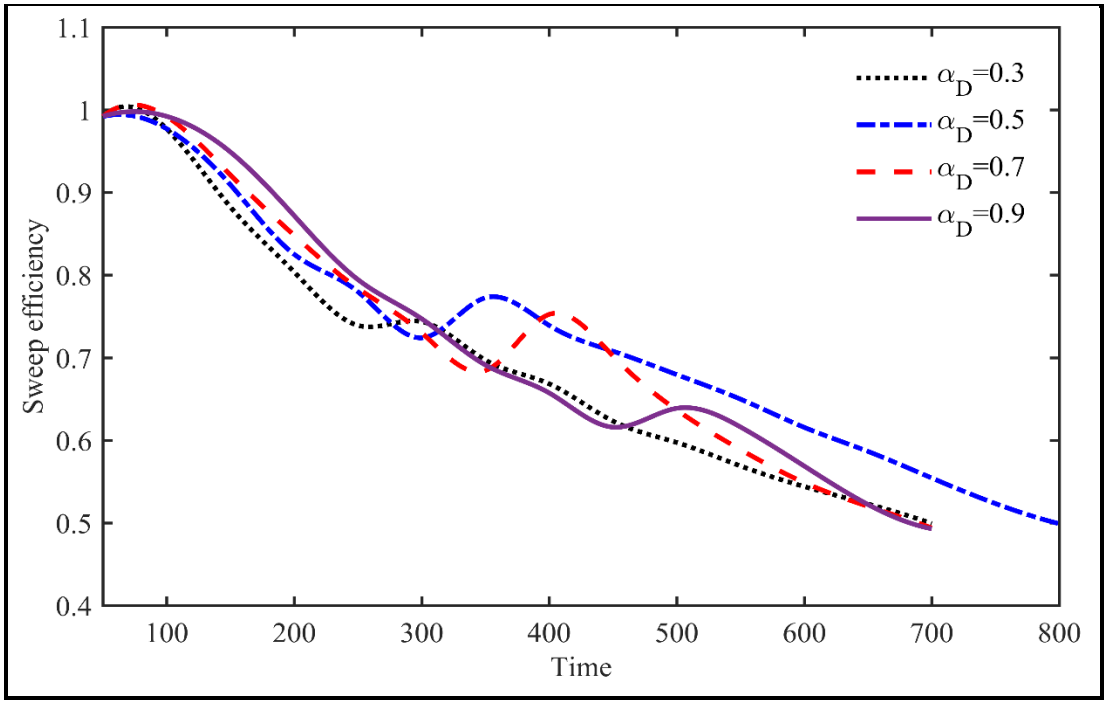

Fig. 27.a. The effect of the dispersion ratio (α_D) on the sweep efficiency $\beta_C = 3$ and $\beta_T = -1.5$.

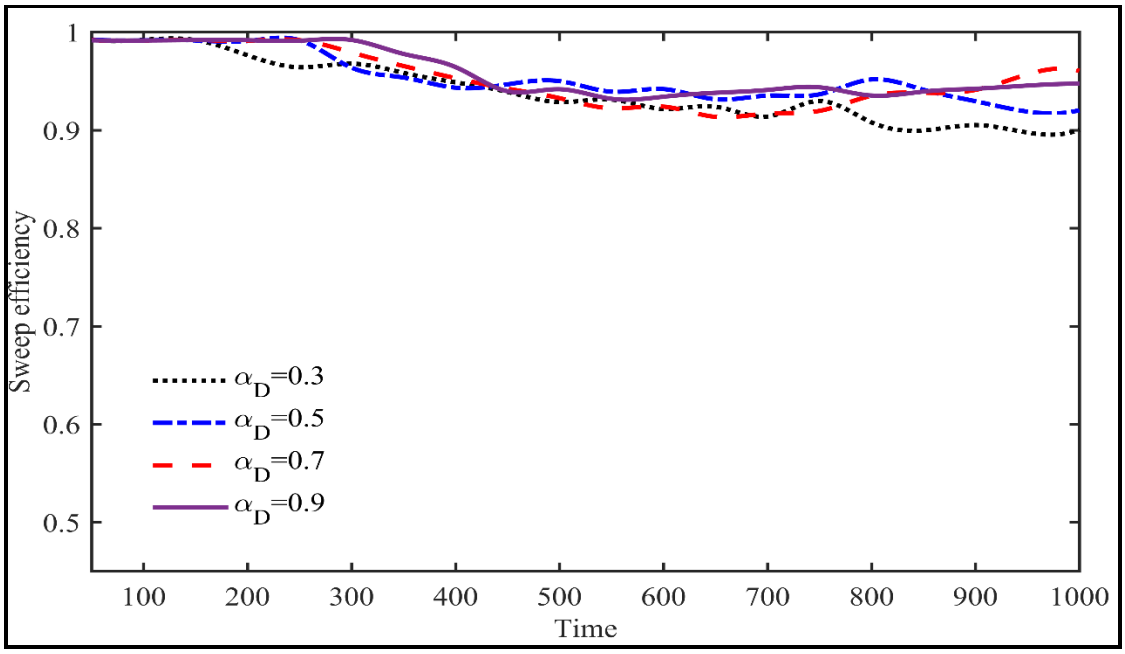

Fig. 27.b. The effect of the dispersion ratio (α_D) on the sweep efficiency $\beta_C = -1.5$ and $\beta_T = 3$.

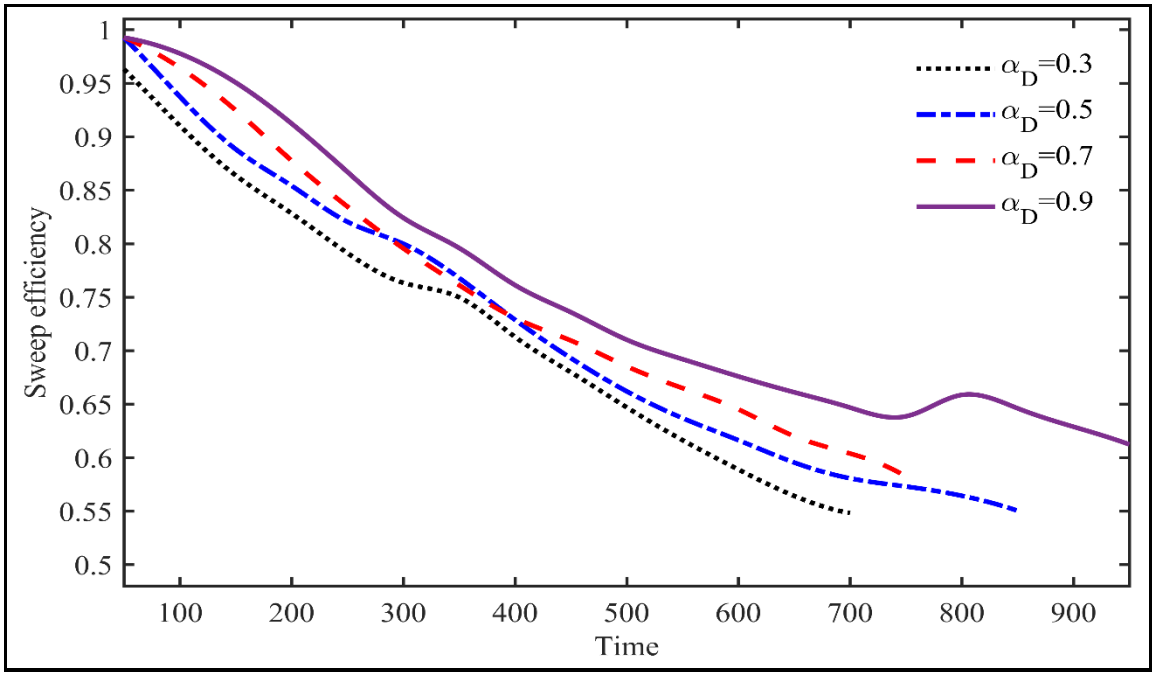

Fig. 27.c. The effect of the dispersion ratio (α_D) on the sweep efficiency $\beta_C = \beta_T = 1.5$.

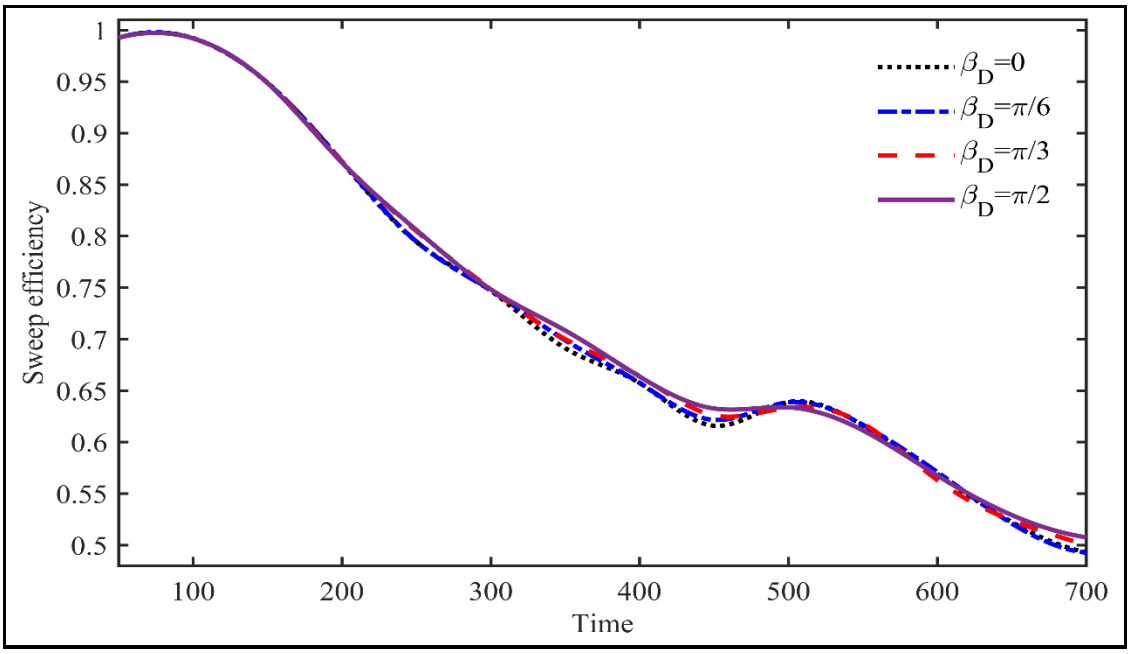

Fig. 28.a. The effect of the dispersion angle (β_D) on the sweep efficiency $\beta_C = 3$ and $\beta_T = -1.5$.

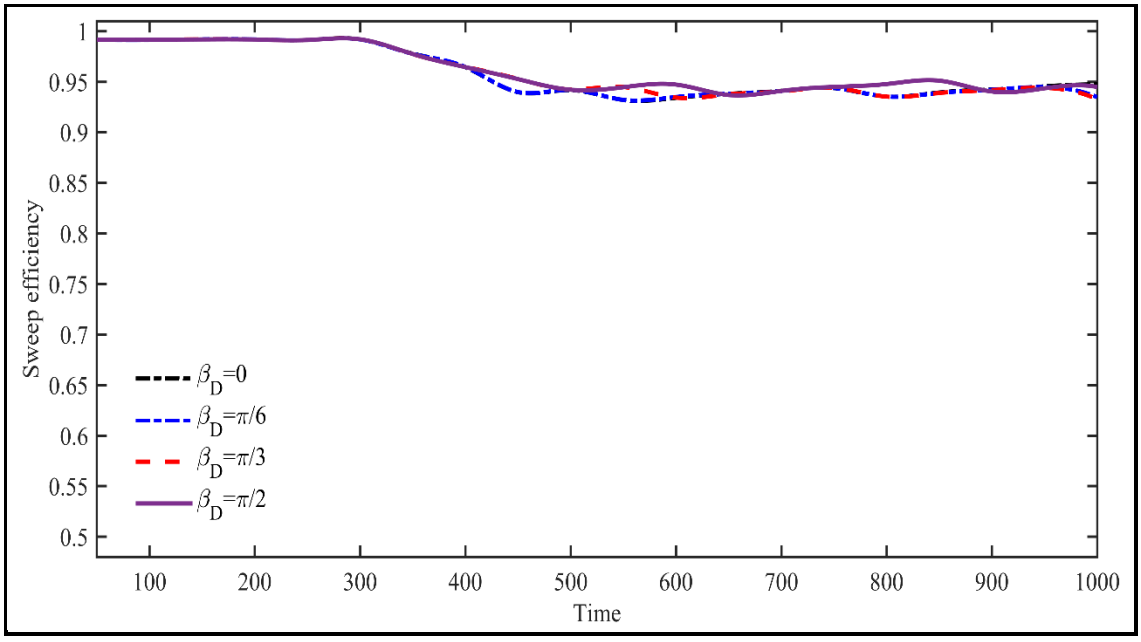

Fig. 28.b. The effect of the dispersion angle (β_D) on the sweep efficiency $\beta_C = -1.5$ and $\beta_T = 3$.

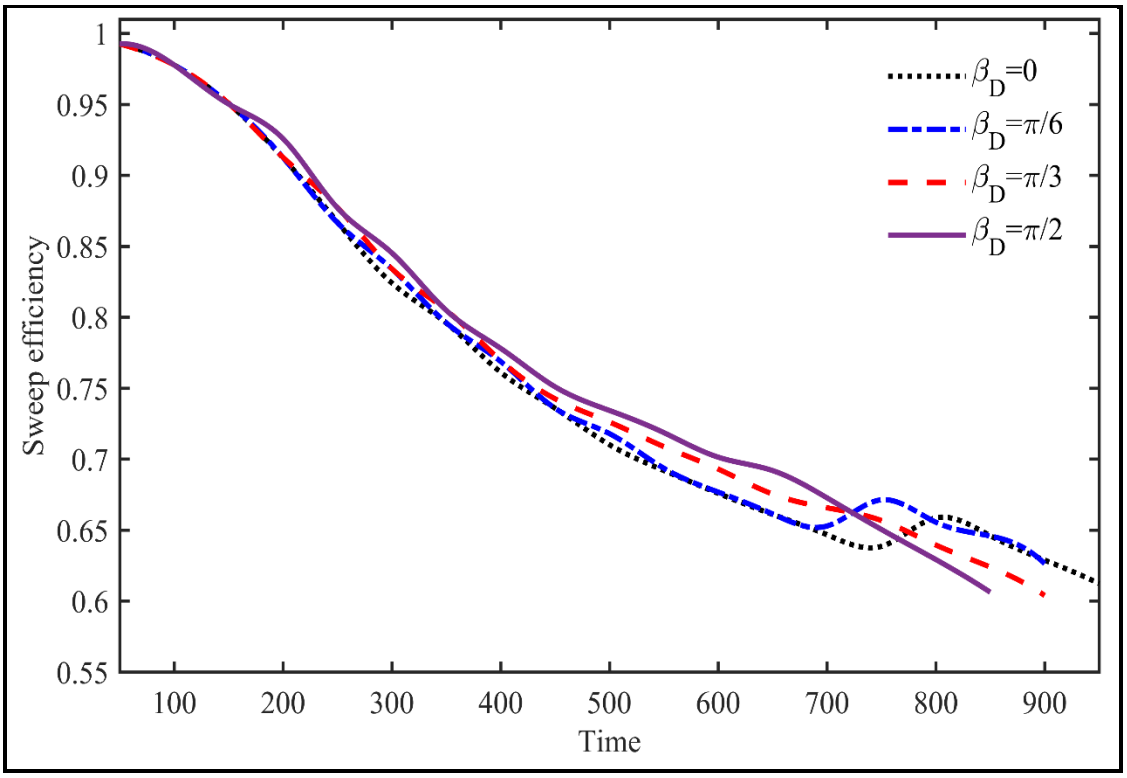

Fig. 28.c. The effect of the dispersion angle (β_D) on the sweep efficiency $\beta_C = \beta_T = 1.5$.